DOE/ER/45337--T5

Fundamental Studies of Stress Distributions and Stress Relaxation in Oxide Scales on High Temperature Alloys

DE-FG02-88ER45337

submitted to
U. S. Department of Energy
Office of Basic Energy Science

by

David A. Shores
James H. Stout
William W. Gerberich

University of Minnesota
Corrosion Research Center
221 Church Street
Minneapolis, MN 55455

June 1993

I. INTRODUCTION

Stresses which develop during scale growth at high temperature, or during temperature changes, can lead to scale fracture, buckling and spallation; subjecting the underlying metal to renewed oxidation. While the existence of these stresses is well established, they have been largely ignored from an alloy design perspective, i.e., no alloy has been designed in which stress minimization was an important design consideration. This is due, in part, to the lack of fundamental understanding of oxidation induced stresses and the factors which control them. On the other hand, high temperature alloys must achieve moderate-to-low stresses to survive thermal cycling; successful alloys have been identified through empirical testing.

Stresses encountered during the oxidation process can be broadly categorized as either growth or thermal stresses. Thermal stresses, also called thermal mismatch stresses, are generated during temperature changes as a consequence of maintaining adherence between the oxide and metal, which have different thermal expansivities. The source of the thermal stress is clearly defined and the magnitude of the stress can be predicted using existing mathematical models.[1-3] Growth stresses, on the other hand, arise from several different sources including epitaxy, concentration gradients, vacancy gradients, volume changes and geometrical considerations. The predominant stress source varies with the metal/oxide system and the oxidation parameters such as temperature, time and oxidant. In most cases the major source of growth stress is the volume change which must be accommodated upon converting metal to oxide. Numerous models have been derived to model growth stresses based on the Pilling-Bedworth ratio.[4-12] These models suffer from a lack of detailed data on the stresses, how they are distributed and transferred, and how they develop and evolve during oxidation. They have not yet reached the level of sophistication required to accurately predict the stresses produced during the oxidation process. The work performed under this contract is an attempt to advance the state of knowledge in this important area

This report summarizes a three-year study of stresses that arise in the oxide scale and in the underlying metal during high temperature oxidation and of scale cracking as a result of these stresses. We have developed and applied *in-situ* X-ray diffraction techniques to measure strains during oxidation at temperatures of over 1000°C on pure metals. We have used acoustic emission to observe scale fracture during isothermal oxidation and cooling, and we have, for the first time, applied a statistical analysis to infer mechanical aspects of cracking. We have developed and applied a microscratch technique at room temperature to make a first measurement of the fracture toughness of the scale/metal interface. Finally we have made a

preliminary evaluation of a theoretical model of the development and relaxation of stresses in the scale and metal substrate during oxidation. This report contains three major sections which summarize the main results of our studies on (a) strain measurements by X-ray diffraction, (b) observation of the mechanics of scale cracking by acoustic emission and microscratch measurements, and (c) modeling of oxidation-induced stresses. A much more detailed account of the experimental techniques and of the experimetal results and interpretations is contained in the several reprints and pre-prints of publications which are attached as an appendix.

II. MEASUREMENTS OF OXIDE SCALE STRESSES BY X-RAY DIFFRACTION

One of the primary goals of our research was to implement an *in situ* technique of x-ray diffraction proposed by Stout, et al.[13] whereby selected X-ray lattice parameters are used as high temperature strain gauges. We have succeeded in this goal; the experimental details are described by Goedjen and by Stout, et al.[14, 15] and particularly by Goedjen et al.[16] which is appended to this proposal.

Overview of Diffraction Experiments

Briefly, our laboratory procedure begins by determining, by x-ray diffraction, the unit cell parameters of the metal or alloy substrate of interest at room temperature. These measurements are taken as the reference values (d_o) for the zero strain state. The substrate is then heated by an external furnace to the temperature of interest where the x-ray measurements are repeated. The heating is done in an N_2/H_2 gas mixture in an effort to minimize oxidation. The high temperature values define the thermal strain , d_{th} (= $(d_T - d_o)/do$) , of the substrate over the range of temperature, typically 900 - 1000°C. While at constant temperature, the gas stream is switched over to pure oxygen and an oxide scale begins to develop on the substrate metal. The x-ray parameters of the metal are monitored in about 5 minute intervals during and after the gas switchover. Typically, but not always, the metal goes into extension relative to d_{th} as the oxide scale develops. The lattice parameters of the newly - formed oxide scale are also monitored continuously as soon as sufficient thickness is developed for measurement. This scale is typically, but not always, in a state of compression relative to d_{th} of the oxide. The value of d_{th} for the oxide cannot be determined in this particular experiment because the lattice parameters of the newly - formed oxide are always influenced by the substrate to which it is attached. Therefore d_{th} of the oxide must be determined in a separate experiment.

The experiment proceeds at high temperature for 6-8 hours until a scale thickness of 2-10 microns is attained. The isothemal growth strains for both oxide and substrate are determined during this time. The substrate and attached oxide is then furnace - cooled to room temperature

where the X-ray measurements are again made in order to evaluate residual strains. These strains represent the combined effects of stresses developed during oxide growth at high temperature and stresses that develop during cooling. The residual strains are rarely zero, and nearly always different in magnitude and sometimes in sign than either the independently measured isothermal growth or cooling strains. Of particular significance is that by these experiments we are able, for the first time, to separate the growth and cooling components of the final residual stress.

We have applied this experimental technique to the oxidation of two metals, namely Ni and Cr. Both have been well studied and residual strain measurements on Ni/NiO and Cr/Cr_2O_3 have been made by many authors. The origin of those strains, however, has never been clearly established. The behavior during oxidation of these two metals is in detail different, and those differences will be discussed below. But based on the experiments conducted to date, some general relationships have emerged that we believe are broadly applicable to other metal/oxide systems as well.

1. Isothermal growth stresses, usually compressive in oxides and tensional in the substrate metal, are a significant component of residual stress.
2. Isothermal growth stresses develop rapidly and reach maximum values that are probably controlled by the high temperature yield strength or creep of the substrate metal or of the oxide.
3. The determination of room temperature residual strains alone reveals little about the actual strain history of the sample.
4. The mechanism by which isothermal growth and cooling strains are relaxed appears to be the same for polycrystalline and single crystal substrate materials,.

None of these relationships could have been identified without an experimental system that allowed rapid, *in situ* , evaluation of elastic strains in both the metal and oxide scale.

Evaluation of Ni/NiO Oxidation Strains

The transmission X-ray diffraction system described above has been used to measure the elastic strains in both the oxide and metal at high temperature during the oxidation of pure nickel. The strain has been measured during oxidation of Ni foils, 6-125 μm in thickness. The transmission mode allows diffraction information to be obtained from the entire oxide and metal volume simultaneously.

Analysis of Stresses from Strains

Determination of the stress state from X-ray diffraction measurements is based on the $Sin^2(\Psi)$ equation, Eqn.(1)[17-19] which describes the elastic strain, measured in any direction, as a function of the six unique components of the stress tensor, σ_{ij}. The orientation of the diffracting plane is described by Ψ and ϕ; Ψ is the angle between the plane of the sample and the

diffracting plane, or alternatively, the angle between the normal to the diffracting plane and the plane of the sample. The measured stain is also a function of the Young's modulus, E, and Poisson's ratio,υ.

$$\varepsilon_{\phi\Psi} = \frac{(1+\upsilon)}{E}\{\sigma_{11}\cdot\cos^2(\Psi) + \sigma_{12}\cdot\sin^2(2\phi) + \sigma_{22}\cdot\cos^2(\phi) - \sigma_{33}\}\cdot\sin^2(\Psi)$$
$$+ \frac{(1+\upsilon)}{E}\{\sigma_{13}\cdot\cos(\phi) + \sigma_{23}\cdot\sin(\phi)\}\cdot\sin(2\Psi)$$
$$+ \{\frac{(1+\upsilon)}{E}\cdot\sigma_{33}\frac{\upsilon}{E}(\sigma_{11} + \sigma_{22} + \sigma_{33})\} \qquad [1]$$

Several assumptions can be made to reduce the number of unknowns, simplifying determination of the stress state. First, by restricting the measurements to thin oxide scales and metal substrates a plane stress state such that, $\sigma_{13} = \sigma_{23} = \sigma_{33} = 0$, can be asssumed. Secondly, the oxide and metal are assumed to be homogeneous, isotropic and randomly oriented, such that an equiaxial in-plane stress condition can be assumed, $\sigma_{11} = \sigma_{22} = \sigma_{||}$, where $\sigma_{||}$, is the in-plane stress. Under these conditions the σ_{12} shear stress must be 0. Equation (1) then reduces to

$$\varepsilon_{\phi\Psi} = \frac{\sigma_{||}}{E}[(1+\upsilon)\cdot\sin^2(\Psi) - 2\upsilon] \qquad [2]$$

That is, the in-plane stress can be determined form a single strain measurement made at any Ψ angle. Under plane-stress conditions, the in-plane stress can be determined from the slope of a graph of measured strain versus $\sin^2(\Psi)$.

Conventional diffractometry, and $\mathrm{Sin}^2(\Psi)$ measurements, are made in the reflection mode. While this technique has been successful in determining the oxide stress, it has met with only limited success in measuring the stress state in the underlying metal. Presumably, this is due to the limited signal intensity from the underlying metal due to absorption of the beam by the oxide scale. Stress gradients within the metal can also complicate interpretation of the results.

The stress state of the metal is also an important element of the total stress state of the system. Plastic yield and creep of the metal substrate may, in fact, determine the stress state of the oxide. Information from the oxide and metal can be obtained by performing the measurements at Ψ=90°, operating in a transmission mode. At Ψ=90° the diffracting planes lie perpendicular to the plane of the sample, Eqn.(2) reduces to:

$$\varepsilon_{\phi\Psi}\Big|_{\Psi=90^\circ} = \frac{(1-\upsilon)}{E}\sigma_{||} \qquad [3]$$

In the transmission mode, the diffraction signal is generated from throughout the oxide and metal, producing an average measurement of the strain in both.

Experimental Procedure

In-situ System

A high temperature X-ray system which operates in the transmission mode has been constructed to make *in-situ* elastic strain measurements in both the oxide and metal. A detailed description of the system has been presented elsewhere.[15] The principle components of the system are a Mo rotating anode X-ray source, a quartz crystal focusing monochromator, a pinhole collimator, a high temperature furnace and specimen stage and a Position Sensitive Detector (PSD). The PSD allows diffraction information to be collected over a radius of 12° without repositioning, enabling expedient data collection. The diameter of the final beam at the specimen is approximately 500 μm. The resolution of the system, which is determined primarily by the detector and associated electronics is approximately $\pm$ 0.02% strain.

Oxidation experiments were performed on Ni (99.99%) foils from 25 to 125 μm in thickness. The foils were recrystallized prior to oxidation for 6 hrs at 1100°C in a N_2-10%H_2 atmosphere and subsequently furnace cooled over a period of approximately 10 hours.

The lattice strain is determined from the diffraction peak displacement relative to the unstrained position. The total lattice strain, ε, is calculated using the equation:

$$\varepsilon_{total} = \frac{d(T)-d_o}{d_o} \qquad [5]$$

where d_o is the stress-free lattice spacing of the oxide or metal at room temperature. The total measured strain also reflects the normal thermal expansion strain of the material. The residual strain, which reflects the growth and thermal expansion strain of the oxide and metal, is obtained by subtracting the thermal expansion from the total measured strain.

$$\varepsilon_{residual} = \varepsilon_{total} - \varepsilon_{thermal} \qquad [6]$$

The experimentally measured thermal expansion of NiO is consistent with results reported by Taylor.[20] The room temperature value of d_o for NiO were also determined by examining the oxide scales removed from oxidized samples. The d_o values of NiO, measured using the *in-situ* system and Debye-Scherrer precision lattice parameter techniques, were equivalent to the ASTM d-spacing values.

Results for Ni/NiO Oxidation Strains

In-situ oxidation

Experimental results from a 25 μm Ni foil provide a represenattive example of the behavior of the Ni/NiO system during oxidation. The residual strain versus time is presented in **Fig.** 1. The results are reported in terms of strain rather than stress due to the lack of reliable modulus data for the oxide over the temperature range of interest.

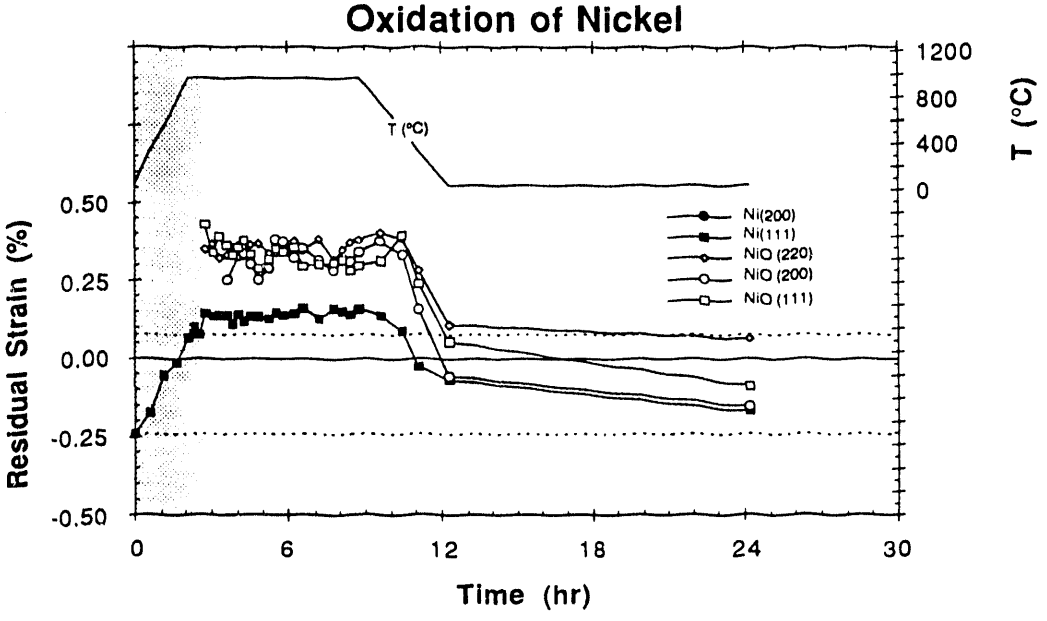

Fig. 1. The residual strain measured during oxidation of a 25 μm Ni foil. The foil was heated to 940°C in N_2-10%H_2 (shaded region) before switching to O_2 (unshaded) The dashed lines indicate the metal strain prior to heating and the metal strain just prior to the introduction of oxygen.

Despite being annealed, a compressive residual strain of -0.25% was measured in the Ni prior to heating and oxidation. At the oxidation temperature, but prior to the introduction of O_2, a tensile strain of 0.075% was measured in the metal relative to the strain-free thermal expansion of Ni. Immediately upon introduction of O_2, an increase in tensile strain of approximately 0.075% was observed in the metal. Significant residual tensile strains of 0.4% were measured in the oxide immediately after introduction of oxygen. Measureable oxide peaks, which reflect a significant residual tensile strain of 0.4%, were observed immediately after introduction of oxygen. The oxide and metal strain remain relatively constant over the duration of the oxidation period. Upon cooling, a residual compressive strain of -0.17% was measured in the metal at

room temperature. While the metal strain measured after oxidation is compressive when measured relative to the ASTM d-spacing, the strain is tensile relative to the initial metal strain measured prior to heating. The residual room temperature oxide strain measured in the NiO (200) and NiO (111) reflections is also compressive. A tensile residual room temperature strain was measured in the NiO (220) reflection; this reflection, however, is very weak and statistically less significant than the NiO (200) and NiO (111) reflections.

Strain measurements were also performed on Ni foils, 50 and 125 μm thick, to examine the effect of substrate thickness on the stress state of the system. In general, the metal exhibits some capacity for stress relaxation and in general has lower residual strains during oxidatiom. The oxide strains, however, remain approximately the same, regardless of metal thickness in the range studied.

Ex-Situ Results - $Sin^2(\Psi)$ measurements

Conventional $Sin^2(\Psi)$ experiments (in reflection) were performed at room temperature on a number of samples which had previously been examined using the transmission technique. The $Sin^2(\Psi)$ results for the oxidized 25 μm Ni foil which previously examined using the *in-situ* technique (Figure 1) provide a representative example of these results. A compressive residual stress of -85 MPa was measured in the oxide at room temperature, **Figure 2**. The in-plane stress was calculated from Eqn.2 using a Young's modulus of 260 GPa and υ=0.4. The stress is equivalent to an in-plane strain of -0.046%. The linear conformation of the data clearly illustrate that a plane stress state is operative in the oxide.

The $Sin^2(\Psi)$ results, measured at room temperature, for the underlying Ni are presented in **Fig. 3**. The weighted linear regression analysis yields an in-plane residual stress value of -30 MPa, as indicated by the slope of the line. The stress was calculated using a Young's modulus of E = 205 GPa[21] and υ = 0.31. The stress is equivalent to an in-plane strain of -0.02%. The compressive stress measured in the metal and oxide is consistent with the room temperature residual strains measured in the *in-situ* experiments. A significant departure from the plane stress conformation is observed in the metal.

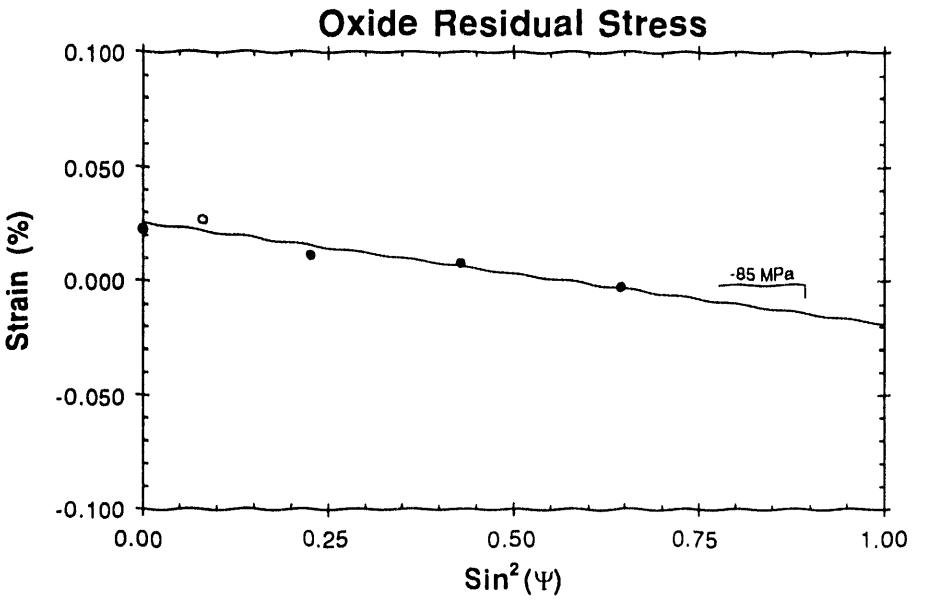

Fig. 2. $Sin^2(\Psi)$ results, measured at room temperature, for the oxide scale formed on the 25 μm Ni foil after 6 hours of oxidation at 940°C in oxygen. The open and closed circles correspond to negative and positive values of Ψ, respectively. The measured strain of -85 MPa corresponds to a strain of -0.046% .

Discussion of Ni/NiO Oxidation Strains

The compressive residual room temperature strains measured in the NiO scale are consistent with those obtained by other investigators using conventional *ex-situ* measurement techniques.[22-25] The residual tensile strains measured in the scale at the oxidation temperature are, however, inconsistent with the conventional Pilling-Bedworth views which suggest that a compressive growth stress should be observed in the oxide. Tensile strains have been reported in oxide scales at high temperature by Liu[26] in the Ni/NiO system and by Bennett[25] in the Cr/Cr_2O_3 system. The elastic strains in both the oxide and metal remains relatively constant during the oxidation period, suggesting that yielding or creep has occurred either in the oxide, or more likely, in the metal.

The measured tensile oxide growth strains may be related more to the growth mechanism which leads to the observed duplex NiO scale than to Pilling-Bedworth considerations. Ueno[27] demonstrated that a complex stress state can exist within the oxide such that each layer of the duplex scale can support a different stress. The analysis of our data is further complicated by the large fraction of metal consumed during oxidation.

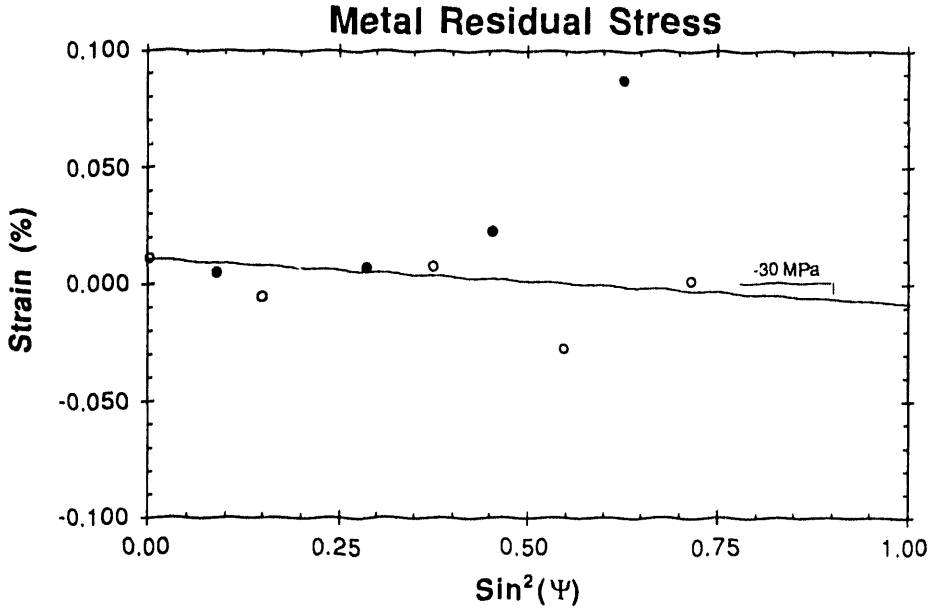

Fig. 3. $Sin^2(\Psi)$ results, measured at room temperature, for the 25 μm Ni substrate after 6 hours of oxidation at 940°C in oxygen. The open and closed circles correspond to negative and positive values of Ψ . The measured stress of -30 MPa corresponds to a strain of -0.02% .

An apparent imbalance of forces is present in the Ni/NiO system at room temperature. Balance of forces requires that the in-plane stresses sum to zero across the thickness of the system. The compressive residual oxide strain measured at room temperature must be balanced by a tensile metal strain, yet compressive strains were measured. At the oxidation temperature tensile strains are observed in both the oxide and metal. Upon cooling, compressive strains are observed in the oxide and metal. This anomaly has also been observed at room temperature by several other investigators.[28-30] It is believed that the observed behavior is due to the departure of the metal from a plane stress equiaxial stress state.

The large grain size of the Ni, 50-100 μm, limits the number of grains within the X-ray beam; the number of grains in diffracting condition is even more restricted. In general the stress will vary from grain-to grain within the metal. Such variations were observed using conventional diffractometry on the annealed foils.[14] When the diffraction information emanates from a large number of grains, the variations in strain and elastic properties are averaged and the metal behaves more like an isotropic homogeneous material despite the local anisotropy among individual metal grains. When a limited number of metal grains are diffracting, the

measurements do not represent a broad average. The homogeneous isotropic condition assumed in deriving Eqns. (1) and (3) is not met. Locally, each grain may depart from the plane stress equiaxial condition and the measured strains cannot be used as an indication of balance of forces between the oxide and metal. The behavior of the metal indicates that the measured metal strains are derived from contributions from each of the six stress components and cannot be determined from a single strain measurement, but require use of the full $Sin^2(\Psi)$ method. The fine grain size of the oxide insures that a large number of grains are in diffracting condition such that the measured oxide strains provide a broad average.

The maximum measured strains are established almost immediately upon introduction of oxygen and remain constant over the duration of the oxidation period. The rapid increase in strain upon introduction of oxygen is consistent with observations made by other investigators using the flexure technique.[31, 32] As oxidation proceeds the growth stresses are expected increase according to several models, yet the observed strain remains constant over the entirety of the oxidation period. This behavior is most pronounced in the 25 μm foil, and less pronounced in the thicker 50 and 125 μm foils. The constant strain at temperature suggests that either the oxide, or more likely the metal, has begun to yield or creep. Once yielding occurs, further increases in stress are accommodated by dislocation motion, and no further increase in elastic strain is observed. The yield strength of the metal imposes a limit to the measured strain; this behavior has not been appreciated in the literature, particularly in thermal stress models. Additional elastic strains may develop due to strain hardening; these additional strains, however, would be exceedingly small, especially when considering the limited strain hardening ability of Ni at high temperature. Plastic deformation is manifested by broadening of the diffraction peak and is difficult to quantify with the current X-ray system.

The thicker foils exhibits some capacity for stress relaxation as manifested by the decrease in strain over the duration of the oxidation period. In the thicker foils the strains are distributed over a greater volume of metal, decreasing the average metal strain and reducing the driving force for creep relaxation. During oxidation of the 25 μm foil the growth stresses do not relax due to the rapidly decreasing metal volume available to accommodate and relax such stresses.

Conclusions of Ni/NiO Oxidation Strains

The residual strains in both the oxide and metal have been measured during all phases of the oxidation process using a transmission X-ray diffraction technique. Assuming a plane stress equiaxial condition is operative in the oxide and metal the application of the conventional $Sin^2(\Psi)$ technique is greatly simplified. Under these assumptions the in-plane stress can be expediently determined from a single strain measurement. Tensile strains as high as 0.4% have

been measured in NiO scales during oxidation at high temperature. While compressive stresses are normally associated with the volume increase upon oxidation (Pilling-Bedworth), in this case, the measured tensile strains may be dictated by the growth mode which produces the duplex oxide morphology. The compressive residual oxide strains measured at room temperature are consistent with the superposition of the compressive thermal stress onto the growth stress. The tensile strains measured in both oxide and metal during oxidation, and the compressive strains measured in the oxide and metal at room temperature, after oxidation is complete, are inconsistent with a balance of forces between the oxide and metal based on a simplified stress analysis. The imbalance is ascribed to the departure of the metal from the plane stress equiaxial condition. Under these circumstances the measured strains can not be attributed solely to the in-plane stress; the normal and shear stress components may also contribute to the measured strain. The departure from the plane stress equiaxial condition can be ascribed to the anisotropic behavior of individual grains of the metal. This is clearly evidenced by conventional diffractometry and $Sin^2(\Psi)$ measurements on the metal. In this case the complete $Sin^2(\Psi)$ method must be used to determine the complete stress state of the metal. The *in-situ* results indicate that the strains in the metal and oxide are established almost immediately upon introduction of oxygen and remain constant over the duration of the oxidation period. The constant strain suggest that the elastic limit is quickly reached in the metal. Strain decreases were observed in the thicker foils suggesting that the rate of creep relaxation exceeded growth stress generation.

Evaluation of Cr/Cr_2O_3 Oxidation Strains

The *in-situ* x-ray diffraction system has also been successfully employed to measure the strain during all phases of the oxidation process - heating, isothermal oxidation, and cooling in the system Cr/Cr_2O_3. There are some important differences in these results compared to those previously discussed for Ni/NiO. The thermoelastic behavior of Cr_2O_3 is more complicated than that of NiO because of its rhombohedral symmetry. The thermal expansion of Cr_2O_3 is anisotropic, with the a - axis direction being about 40 % more expandable than the c-axis direction. This means that unlike NiO, diffraction planes such as $(11 \cdot 0)$ in Cr_2O_3 will serve as more sensitive strain gauges than will reflections such as $(11 \cdot 6)$ and $(10 \cdot 4)$. This behavior has important consequences for the development of thermal stresses upon cooling to room temperature because the thermal expansivity of the Cr metal has a value between the a-direction and c-direction expansivities of the oxide. This behavior is apparent in **Fig. 4** where the linear expansivity of the above 3 directions in Cr_2O_3 is compared to the single value for Cr metal. If one now wishes to calculate the thermal stress in either the oxide or the metal using, for example,

the Tien-Davidson[2] formulation , the sign of Δa can be either positive or negative. In detail this means that thermal stresses can be either in compression or in tension depending on lattice orientation of the oxide.

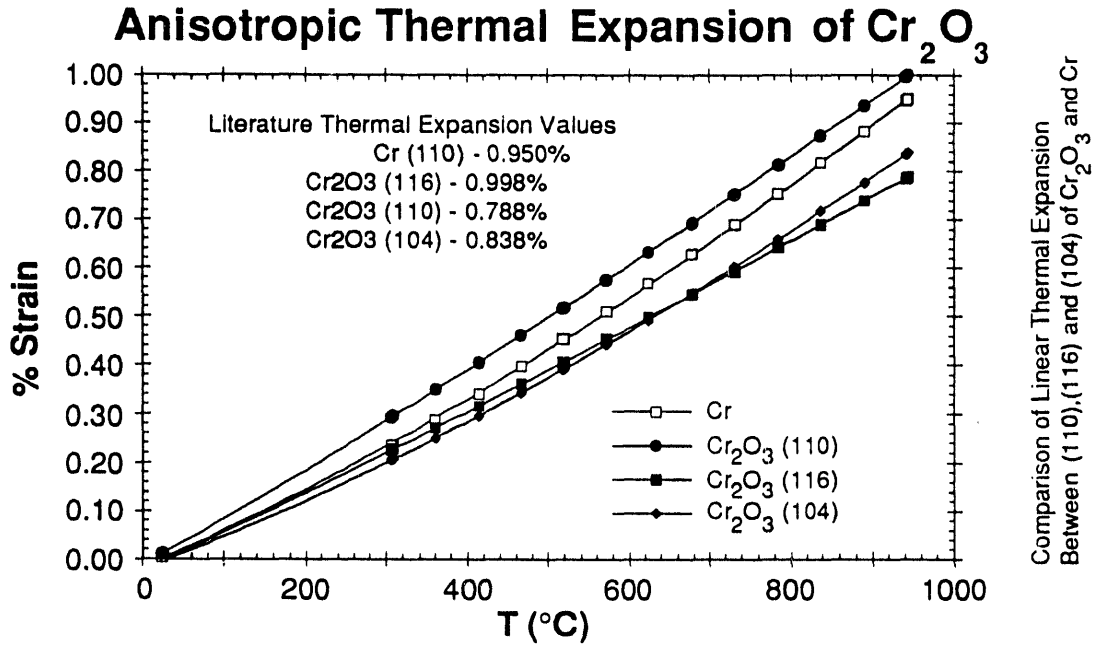

Fig. 4 Measurements of thermal expansion strains for various crystal directions in Cr_2O_3 and chromium.

We have completed oxidation experiments on both polycrystalline and single crystal Cr. The polycrystalline results [15] are similar to those for Ni/NiO in the sense that high temperature growth strains are observed and the maximum strains in the oxide appear to be limited by the yield strength of the metal. Moreover, the final residual stresses observed in Cr and Cr_2O_3 are a combination of the stresses developed during growth at high temperature and the stresses that develop during cooling. For both Cr/Cr_2O_3 and Ni/NiO it seems clear that by evaluating residual stresses alone, one learns very little about the actual stress history of the system.

A fundamental difficulty in the experimental evaluation of stresses in oxidizing polycrystalline Ni or Cr if they have a relatively coarse grain size, i.e., a grain size such that a few grains (10's of grains) are illuminated by the X-ray beam. There is never a guarantee that the metal grains that are actually in diffracting position are the same grains on which the oxide scale grows. As we have shown for Ni/NiO[14, 16] an apparent imbalance of forces across the metal/oxide interface can result. The only unambiguous solution to this problem is to do

oxidation experiments on oriented slices of single crystals where there can be no doubt that the diffracting substrate is in contact with the oxide scale.

Typical results for the oxidation of single-crystal Cr, oxidized on the (100) face at 940°C, are illustrated in **Fig. 5.** The top line (open circles) in this figure gives the temperature variation of the experiment over time (abscissa). The closed circles represent the behavior of unconstrained Cr metal as determined from a separate experiment. After 2 hours, the metal is fully expanded and remains that way for 5 hours until cooling commences. There is no residual strain after cooling to room temperature. The behavior of oxidizing Cr metal is represented by the square symbols and is clearly different than that of the unconstrained Cr. The constrained metal is in tension at 940°C and remains that way for the duration of the oxidation and during cooling to yield a tensional residual strain.

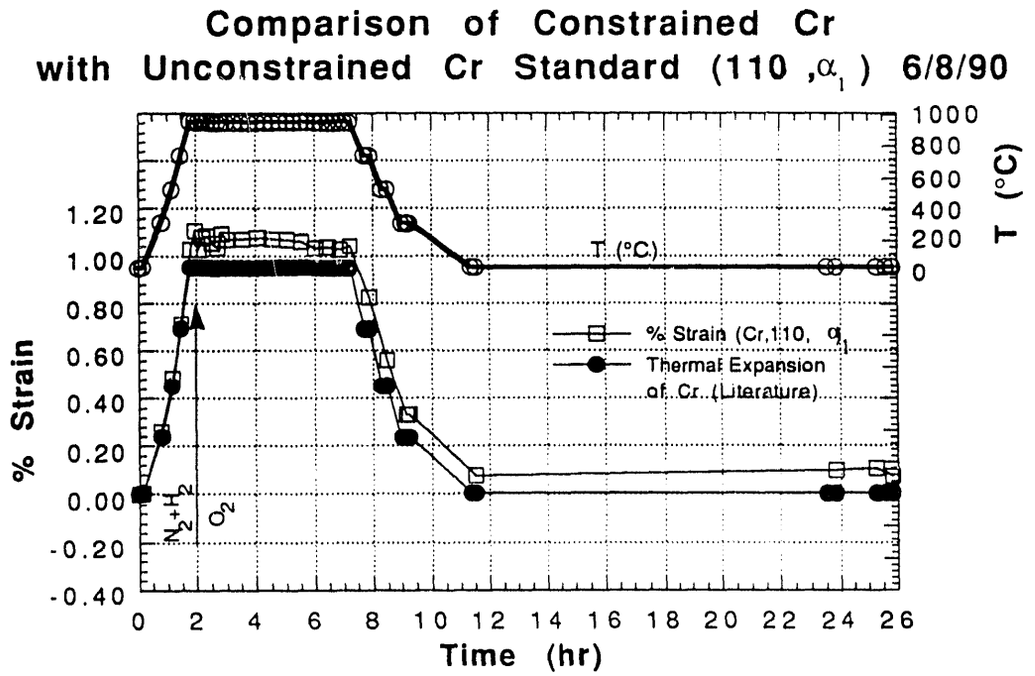

Fig. 5 Comparison of thermal expansion strains in unconstrained Cr metal with thermal expansion strains in Cr that is being oxidized at 940°C.

The oxide, which is observed shortly after the introduction of oxygen, is found to be in compression (relative to unconstrained Cr_2O_3) during the isothermal oxidation. The [11·0] Cr_2O_3 direction (**Fig. 6**) exhibits the greatest compressive strain during growth but upon slow cooling, the evidence for this strain is lost. The reason for this is that during cooling, the [11·0] direction

of the oxide actually contracts faster than does the metal and tensional cooling stresses result. These are opposite in sign to the growth stresses and a near zero residual strain is observed.

The [11·6] and [10·4] directions of Cr_2O_3 are less expandable than the metal and the cooling behavior is quite different. **Figure 7** shows the behavior of the [10·4] direction which is nearly parallel with the c-axis of the rhombohedral structure. The closed circles represent the behavior of unconstrained Cr_2O_3, and the open triangles the behavior of the Cr_2O_3 as it grows on the metal. There is little evidence for growth strains until after about 6 hours when the oxide appears to be in slight compression. During cooling, however, compressional strains develop and for this direction in Cr_2O_3, account for most of the final residual strain which is in compression.

We conclude from these experiments that the relative magnitude of the residual strains in chromia scales grown on single crystal surfaces is due to the pre-existing growth stress and the anisotropic behavior of the thermal expansivity during cooling. Thermal expansion in the [11·0] direction of Cr_2O_3 is greater than that of the Cr substrate and the strains essentially cancell. The thermal expansion in the [10·4] and [11·6] directions of Cr_2O_3 is less than that of Cr and the strains are additive. From an practical standpoint, Cr_2O_3 scales which grow with their c-axes normal to the metal interface should have minimal in-plane sresses and should be more resistant to failure.

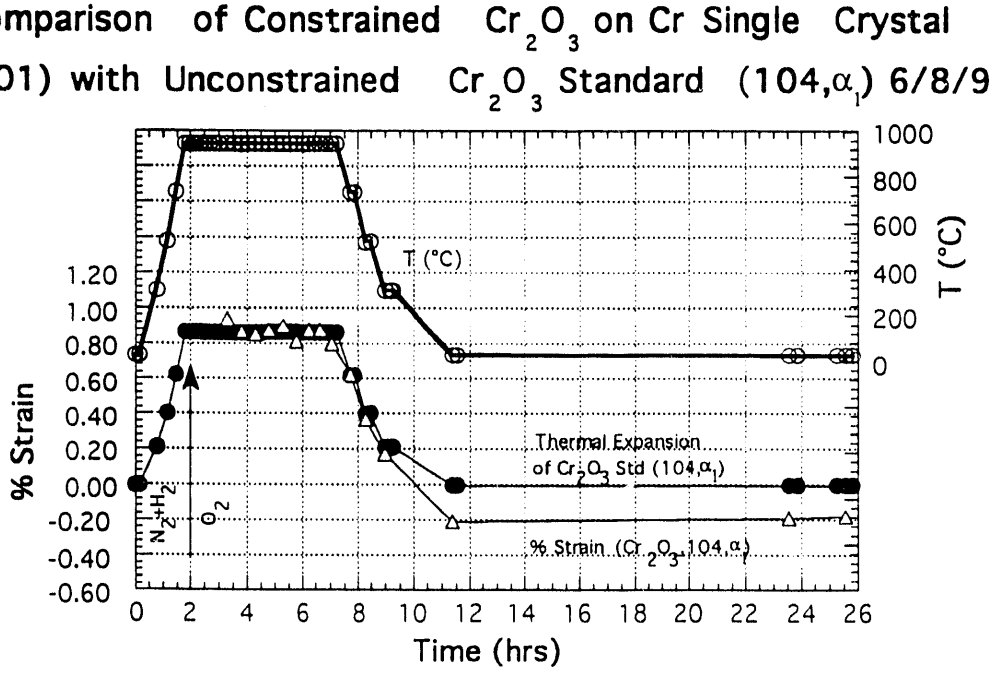

Fig. 6 Comparison of thermal expansion strains in unconstrained Cr_2O_3 with strains in Cr_2O_3 scale formed during oxidation at 940°C in oxygen.

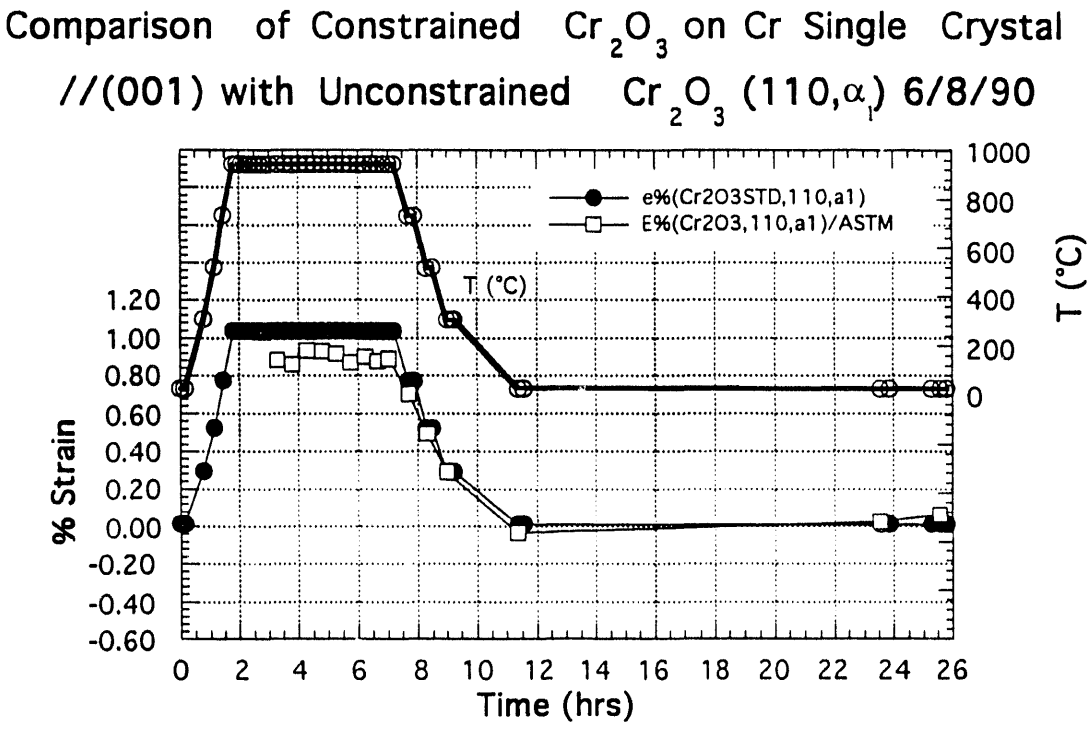

Fig. 7 Comparison of thermal expansion strains in unconstrained Cr_2O_3 with strains in Cr_2O_3 scale formed during oxidation at 940°C in oxygen.

III. OXIDE SCALE CRACKING AND SPALLING

In most cases of oxidation of high temperature alloys, stresses generated in the oxide during isothermal oxidation and during cooling are compressive. H. E. Evans et al[33, 34] have proposed two routes for oxide scale failure. The first one is that the strength of the metal/oxide interface is higher than the compressive fracture strength of the oxide. In this case, a shear crack will be formed within the oxide layer at an early stage. The crack is presumably nucleated at pre-existing defects, and it can penetrate to the metal surface. The formation of this shear crack can result in a geometry which permits tensile cracks to be wedged along the oxide/metal interface leading to spallation. Secondly, if the interface is relatively weak, a crack can propogate along the oxide / metal interface, leading to buckling and eventually to spallation when through-thickness cracks develop in tensile regions at the perimeter of the buckle.

In this section two studies will be described that have used quite different experimental techniques to measure parameters related to oxide scale failure. The first has used *in-situ* acoustic emission to study the cracking and spalling of scales formed on Ni-30Cr alloy and on

304 stainless steel. The second has developed and used a micro-scratch technique to estimate the fracture toughness of the metal / scale interface on Ni / NiO. Both studies point toward a weak interface as the most likely mode of spallation on these materials.

Observation of Scale Cracking by Acoustic Emssion

The purpose of this study was to measure cracking events during the oxidation and subsequent slow cooling of Ni- 30 Cr and 304 stainless steel and to use this data to evaluate models of cracking / spallation. A complete description of the experimental procedures, experimental results and interpretations is given in the attached pre-prints:

Y. Zhang and D. A. Shores, "Measurement of Oxide Scale Cracking and Spalling from 304 Stainless Steel Using Acoustic Emission", in Proc. of Symp. on Oxide Films on Metals and Alloys, Ed. B. R. MacDougall, R. S. Alwitt and T. A. Ramanarayanan, The Electrochemical Soc. 92-22, p. 250-264(1992).

Y. Zhang and D. A. Shores, "Study of Cracking and Spalling of Cr_2O_3 Scale Formed on Ni- 30Cr Alloy", submitted to Oxidation of Metals, April, 1993.

Y. Zhang and D. A. Shores, "Cracking and Spalling of Oxide Scales From 304 Stainless Steel at High Temperatures", submitted to J. Electrochem Soc., June, 1993.

Experimental Procedure (Acoustic Emission)

The experimental procedure is described in the reprints attached. Briefly, alloy coupons were polished through 1 μm diamond paste on a napped cloth. A platinum wire of 0.5 mm in diameter was spot-welded on the sample surface to transfer the stress waves produced by the cracking and spalling of the scale to a piezoelectric AE sensor, which can transduce the elastic strain wave into electric signals. The oxidation experiments were conducted in pure oxygen flowing at 50 cc/min at 1000°C for Ni-30Cr alloy and 800°C for 304 stainless steel. Then samples were furnace cooled to room temperature. The AE data were collected throughout the experiment by an AET 5000 acoustic emission equipment. The AE sensor has a sensitivity of -70 dB referred to 1 volt per microbar. The frequency response of the pre-amplifier is from 1 kHz to 2 MHz. The total amplification of the AET 5000 system was 95.6 dB.

The acoustic emission data is characterized as a packet of high-amplitude waves, called an event; typically an individual crack will produce an event comprised of several waves. The AET 5000 can discriminate the waves in an event and can count the number of the events as a function of time. It can also measure the following parameters of an event: peak amplitude, ringdown count, the number of the individual peaks passing the threshold, the event duration and the rise time. At the beginning of an experiment, an amplitude threshold was set to filter out

mechanical background noise, and an event duration criterion of 20 microsecond was set to filter out electrical noise. After the experiment, the samples with remaining oxide scales were examined by scanning electron microscope (SEM) and energy dispersion analysis of x-rays (EDAX).

Results and Discussion (Acoustic Emisson)

Modeling studies of the oxide scale spallation process show that for flat scales the oxide spalling process is preceded by scale buckling, which occurs when an initial interfacial flaw exists with radius greater than a critical value a_c:[10, 35, 36]

$$a_c > 1.1\ h \left(\frac{E_{ox}}{\sigma_o}\right)^{1/2} \qquad [7]$$

where h is the scale thickness, E_{ox} is the Young's modulus of the oxide and σ_o is the biaxial stress applied to the scale. After buckling, the average compressive stress in the buckled region is reduced, but a stress concentration arises at the perimeter of the buckle. If the interfacial crack exceeds a critical value, a_s, the crack will tend to deflect toward the surface at the crack tip, resulting in spalling. a_s is given by:[10, 35, 36]

$$a_s = 1.9\ h \left(\frac{E_{ox}}{\sigma_o}\right)^{1/2} \qquad [8]$$

Cracking and spalling of oxide scale from Ni-30Cr alloy

The oxidation at 1000°C for 20 hours in pure oxygen flow produced Cr_2O_3 scale about 5 μm thick on the Ni-30Cr alloy. **Figures 8** and **9** show the acoustic emission results of the experiments in which samples were oxidized for 20 hours, then naturally furnace cooled to room temperature or cooled to room temperature by constant cooling rate (about 19°C/hour). The figures show that in the isothermal oxidation stage, a small number of cracking events were collected. This indicates that some growth stress was generated during the isothermal oxidation stage. The isothermal growth stress is expected to be relatively small, however, stress concentration can occur on sample edges and corners, causing cracks there under low average stress. These cracks can provide the through-thickness separation of the scale for later spallation process.

During cooling to room temperature, an additional, and larger component of stress is induced by the different thermal expansion coefficients of the metallic substrate and oxide. Applying Tien and Davidson's model[2], when the ratio of the scale thickness to the sample thickness is very small, the thermal stress is,

$$\sigma_{therm.} = \frac{E_{ox}\Delta T(\alpha_A - \alpha_{ox})}{1-\upsilon} \qquad [9]$$

where ΔT is the cooling amount and $(\alpha_A - \alpha_{ox})$ is the thermal expansion difference between oxide scale and the substrate alloy, υ is the Poisson's ratio. The compressive stress will increase during cooling in proportion to ΔT. The total stress applied to the oxide scale will be the sum of the growth stress and the thermal stress. Therefore, the total stress σ_o in equations (7) and (8) is:

$$\sigma_o = \sigma_{grow} + \sigma_{therm} \qquad [10]$$

Figures 8 and **9** also show that continuous cracking and/or spalling of Cr_2O_3 scale started when the sample was cooled to a certain temperature (about 500°C), indicating that a minimum stress is required to initiate the cracking/spalling process. The extensive cracking and spalling process continued over a temperature range, indicating that the scale does not fracture at a single value of stress. From **Fig. 8** it can also be found that the peak of the time-to-cracking distribution of natural furnace cooling experiment is skewed toward the left. This is because the cooling rate was decreasing with cooling time. When the sample is cooled at a controlled constant rate, the peak was symmetrical or skewed slightly toward the right, as shown in **Fig. 9**

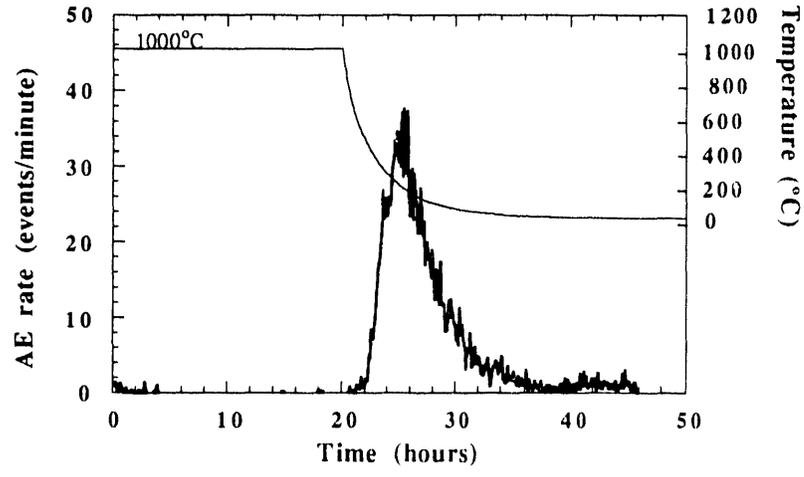

Fig. 8 The AE result of the naturally furnace cooling experimrnt of Ni-30Cr alloy.

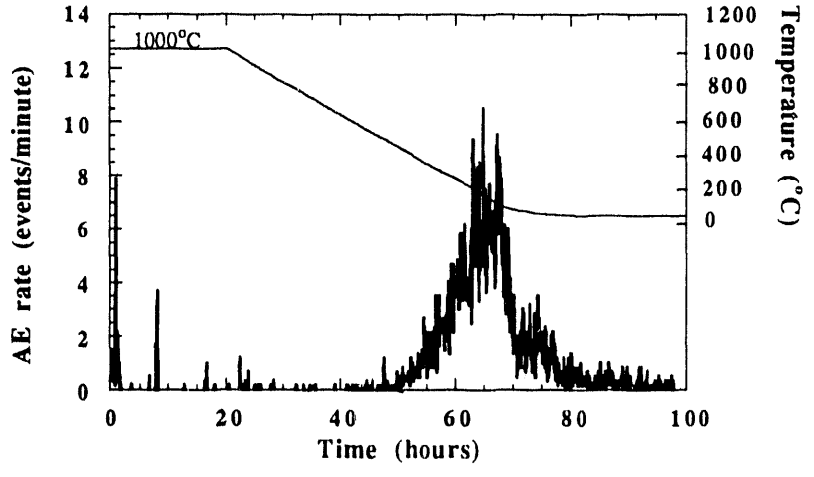

Fig. 9 The AE result of the constant cooling rate experiment of Ni-30Cr alloy.

Scanning electron microscopy of a fractured cross section of the Cr_2O_3 scales showed two layers: an outer layer with coarse columnar grains and a thin inner layer with fine equiaxed grains. Many buckled regions were found on the remaining scale, and through-thickness cracks were only found on the top of buckled regions or along the perimeter, as shown in **Fig. 10** This morphology suggests that the scale spalled predominantly via the second mode (Route II) proposed by H. E. Evans et al,[33, 34] i.e., the interface between Cr_2O_3 scale and Ni-30Cr substrate is relatively weak.

Equation (7) predicts the critical half length of the interfacial flaws required to produce buckling. If σ_0 is spatially uniform, the intrinsic distribution of the fracture stresses (as inferred from a distribution of fracture events) is mainly derived from a distribution of the sizes of the interfacial flaws. The intrinsic distribution of the fracture stresses can be indirectly measured by AE, therefore we can use equation (8) to calculate the distribution of the sizes of spalled areas based on AE data, and equation (7)to calculate the distribution of sizes of the interfacial flaws which produced the buckling required by spallations.

As mentioned earlier, *in-situ* strain measurement by x-ray diffraction[37] indicates that the growth stress generated on the Cr_2O_3 scale formed on Ni-25Cr alloy at 950°C is about -550 MPa, if Young's modulus is taken as 273 GPa.[38] We would expect the growth stresses to be similar and in the following calculation, we will take the growth stress σ_{gw} = -550 MPa, the Young's modulus E_{ox} = 273 GPa, $(\alpha_A - \alpha_{ox}) = 1.58 \times 10^{-5}$ (K^{-1}),[38] and $\upsilon = 0.3$. The creep of substrate during cooling and the effect of temperature on E_{ox} and $(\alpha_A - \alpha_{ox})$ have been ignored.

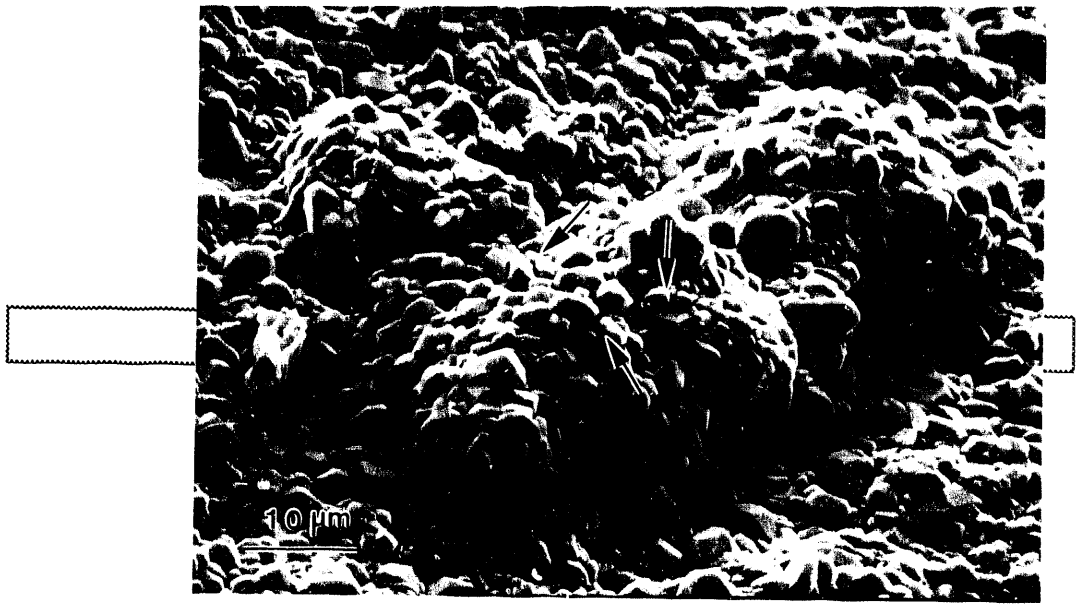

Fig. 10 The SEM micrograph showing a buckled region of the Cr_2O_3 scale formed on Ni-30Cr alloy by 20 hours oxidation at 1000°C, the arrows indicate the cracks running on the top of the buckle.

In our experiment, the number of AE events generated inside a temperature interval can be measured as a function of ΔT. If we take as a simple model that the spalled area is square and each spalling will produce Z AE events, Z-1 from through-thickness cracks along the perimeter of the buckled region and 1 from the buckling, then the number of interfacial flaws to be spalled can be one Zth of the AE events number, where Z would be 5 for a square spallation area. Z might typically range from 5 to 7 or 8. Combining equation (7) and equation (8) and rearranging:

$$\Delta T = \left\{ 14.44 \frac{E_{ox} h^2}{(2a_s)^2} - \sigma_{gw} \right\} \frac{(1-\upsilon)}{E_{ox}(\alpha_A - \alpha_{ox})} \qquad [11]$$

Using equation [11] we can obtain the number of spalled areas with size $2a_S$, N, as a function of $2a_S$:

$$N = F(2a_S) \qquad [12]$$

where

$$F(2a_S) = f\left(\left\{ 14.44 \frac{E_{ox} h^2}{(2a_S)^2} - \sigma_{gw} \right\} \frac{(1-\upsilon)}{E_{ox}(\alpha_A - \alpha_{ox})} \right)$$

Using equation (12) we can convert the measured distribution of AE events in the temperature domain to the distribution of the sizes of spalled areas. By combining equation(7) and equation (8) we can convert the size distribution of spalled areas into the size distribution of interfacial flaws.

Figures 11 and 12 show the calculated size distributions of spalled areas and the calculated interfacial flaws based on AE data. The bold lines in these figures are the normal distribution curves fitted to the calculated data. The parameters for the distributions are listed in the figures. It can be seen that the curves calculated by equation (12) fit the normal distribution satisfactorily except that the sizes of the spalled areas are truncated at a lower limit.

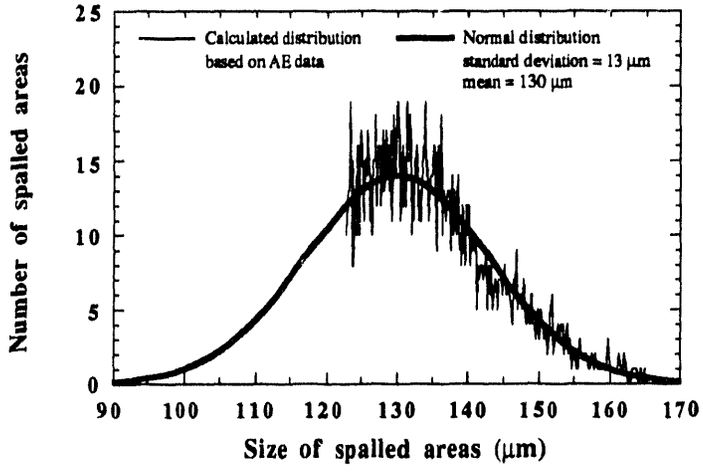

Fig. 11 The calculated size distribution of spalled areas of the naturally furnace cooled experiment of Ni-30Cr alloy.

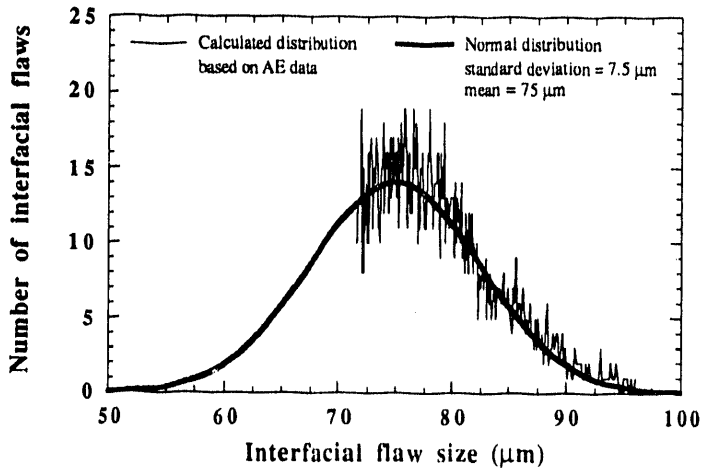

Fig. 12 The calculated size distribution of the interfacial flaws of the naturally furnace cooled experiment of Ni-30Cr alloy.

Figure 13 is a SEM measured size distribution of spalled areas. More than 500 spalled areas were measured on the sample. These data fit a normal distribution reasonably well. The average size of spalled areas is about 45 μm, smaller than the calculated average values using equation (12). This difference probably arises because of defects in the scale, whereas the derivation of equations (7) and (8) modeled the delaminated region of the scale as a clamped, smooth, defect-free circular plate.[36, 39] The real oxide scale has defects such as grain boundaries and many small sharp V-notches on the scale surface, as shown by **Fig. 10**. These defects will cause local stress concentrations which make the scale easier to be buckled and spalled. Therefore, an interfacial flaw with a size smaller than predicted by equation (7) can cause buckling. Similarly, the stress concentrations around the perimeter of the buckled region, caused by the oxide grain boundaries and the small sharp V-notches, will make the buckled region spall before the interfacial crack under the buckled region propagates to the size predicted by equation (8).

Cracking and spalling of oxide scale from 304 stainless steel

Samples of 304 stainless steel were oxidized isothermally at 800°C for 20 hours in flowing pure O_2, then were furnace cooled to various temperatures and held for 24 hours. The isothermal oxidation produced a film 3 μm thick scale of spinel . An argon flow was led into the system after the isothermal oxidation to suppress further oxidation during holding. After the

thermal hold the samples were furnace cooled to room temperature. Acoustic emission signals were collected throughout the oxidation experiment.

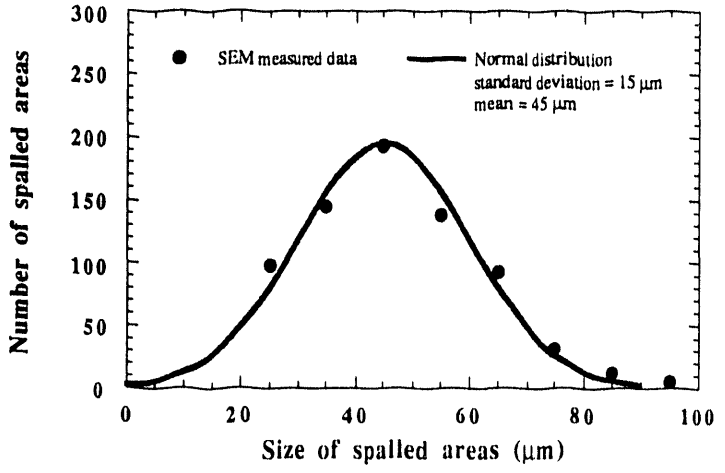

Fig. 13 The SEM measured size distribution of spalled areas for Ni-30Cr.

Figure 14 shows the results of an experiment in which the sample was isothermally oxidized for 20 hours, then furnace cooled to room temperature. As indicated above, only insignificant number of AE events were recorded during isothermal oxidation. The scale started to crack and spall extensively when the sample was cooled below 300°C. As cooling proceeded, the amount of cracking and spalling (represented by the AE events) increased to a peak value around 150°C, then decreased to zero after several hours at room temperature.

For other samples, cooling was interrupted for 24 hours at different temperatures below 300°C. As one example, **Fig. 15** shows the results of an experiment in which the sample was held at 200°C for 24 hours. It can be seen that AE events were initiated at approximately 300°C, as before, but the events stopped when the temperature stabilized at 200°C, implying that the scale fracture process had been stopped. When cooling was resumed after 24 hours, additional events were recorded, giving rise to a steep peak, indicating that the extensive scale cracking and spalling started again at a small additional ΔT.

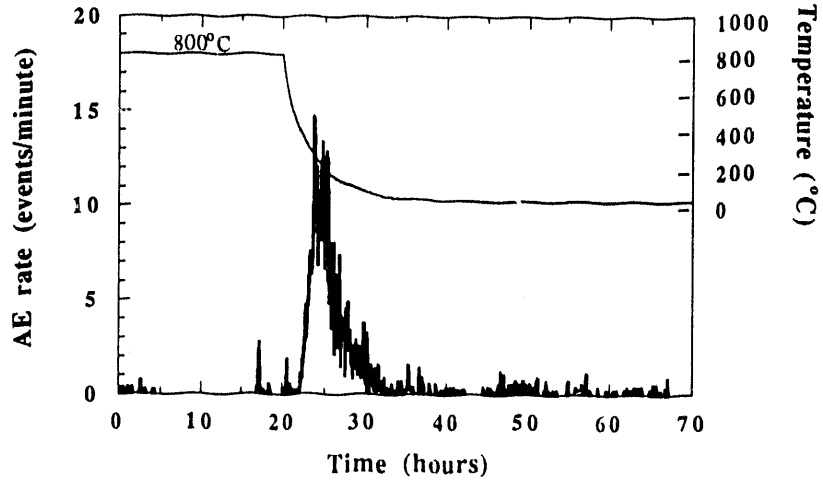

Fig. 14 The AE result of the continuous cooling experiment of the 304 stainless steel.

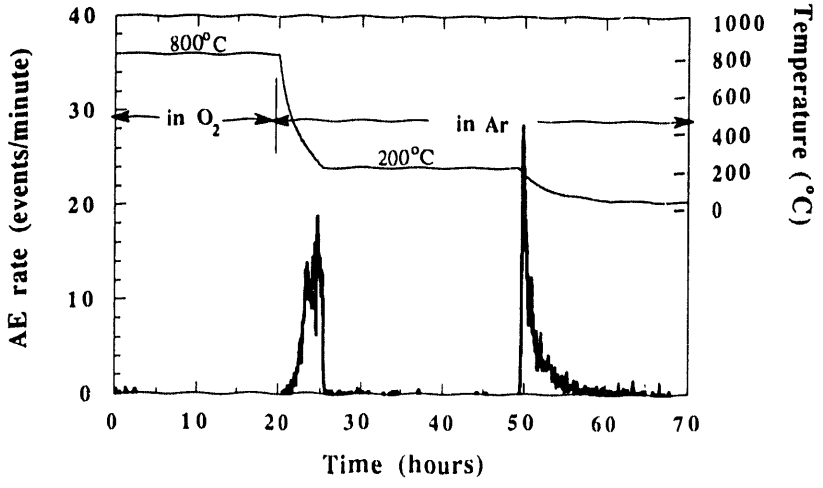

Fig. 15 The AE result of the 200°C holding experiment of the 304 stainless steel.

From the above experimental results it can be seen that extensive cracking and spalling of the scales continued over a range of temperature, indicating that no single value of critical fracture stress applies to the entire specimen, in agreement with the proposal by Evans et al.[40, 41] As he proposed, there will be an intrinsic distribution of the critical strain energy W_f^* across the surface such that some areas will spall at low values of W_f^* and others will spall at high values. The critical strain energy W_f^* is achieved primarily by the stress induced by thermal expansion mismatch during cooling. As ΔT increases, more and more of the distribution will be covered, so that an increasingly larger fraction of the scale experiences a strain energy equal to or higher than W_f^*. The results shown in **Figs. 14** and **15** basically support this proposal except that the acoustic emission was not absolutely stopped when cooling was stopped either at room temperature or at intermediate holding temperatures. These continuing cracks at constant temperature (and hence at constant stress) can not be accounted for by Evans' proposal.

An alternative description may be based on fracture mechanics. Here, the key factor controlling the fracture of brittle materials is the stress intensity factor K, a combination of stress and crack length:[42]

$$K = Y \cdot \sigma \cdot \sqrt{\pi \cdot a} \qquad [13]$$

Rapid crack propagation occurs when K exceeds a critical value, K_C, which can be considered to be the fracture resistance of the scale. From the equation we can see that even at constant stress, K can be increased by increasing the crack length. Under some conditions, i. e., plane strain, a sharp crack and uniform structure of the sample, Y is essentially constant and K_C is an intensive property of the material. Because one or more of these conditions may not be met, K_C may vary with location on the specimen. Therefore, a distribution of cracking events as a function of applied (average) stress could be attributed to a distribution of K_C's.

SEM analysis has shown that the spallation process is preceded by scale buckling, i. e., the spallation was via Route II, as shown in **Fig. 16**.

Elastic buckling requires the pre-existence of an initial separation between scale and substrate with a half crack length, a_c, predicted by equation (1). The interfacial crack under the buckled region will propagate if the following condition is satisfied:[36, 43]

$$K_c^i = h^{5/2} \frac{E_{ox}}{a_c^2} \qquad [14]$$

where K_c^i is the critical stress intensity factor for the growth of an interfacial crack, or the fracture resistance of the interface.

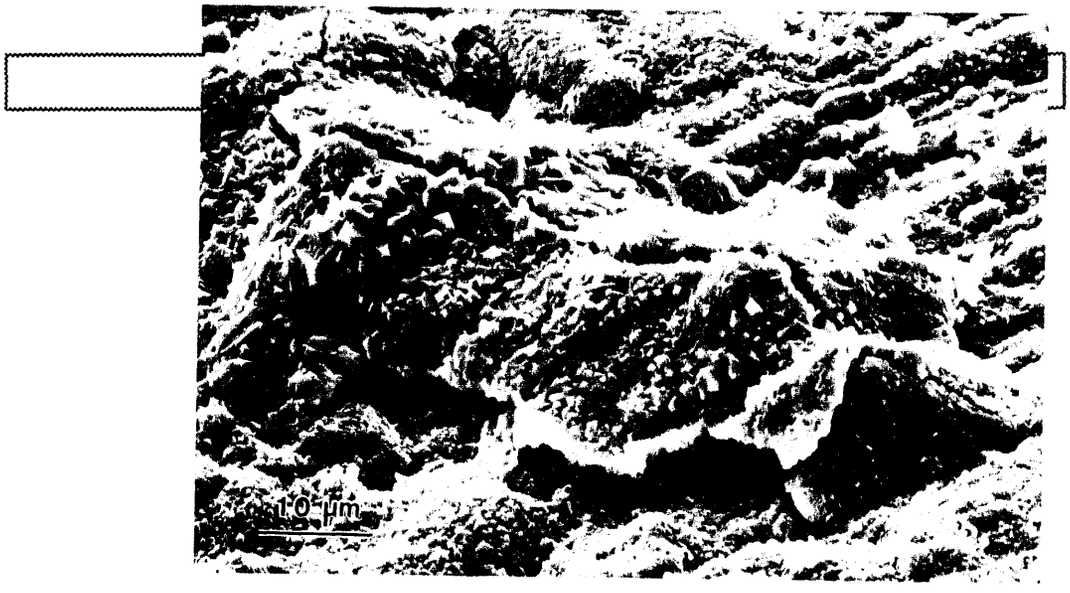

Fig. 16 The SEM micrograph showing buckling and spalling of the oxide scale formed on 304 stainless steel.

As the stress is increased during cooling, buckled regions with the lowest K_c^i will expand first. When the interfacial crack reaches a value a_s predicted by equation [8], the interfacial crack will tend to deflect toward the surface at the crack tip, resulting in spalling. Combining equations (7), (8) and (14):

$$K_c^i = 2.93\, h^{5/2}\, \frac{E_{ox}}{a_s^2} \qquad [15]$$

where a_s can be measured by SEM. The SEM measured size distribution of spalled areas is shown in **Fig 17**. The data can be fairly well fit into a normal distribution with average diameter = 50 μm and standard deviation = 17 μm.

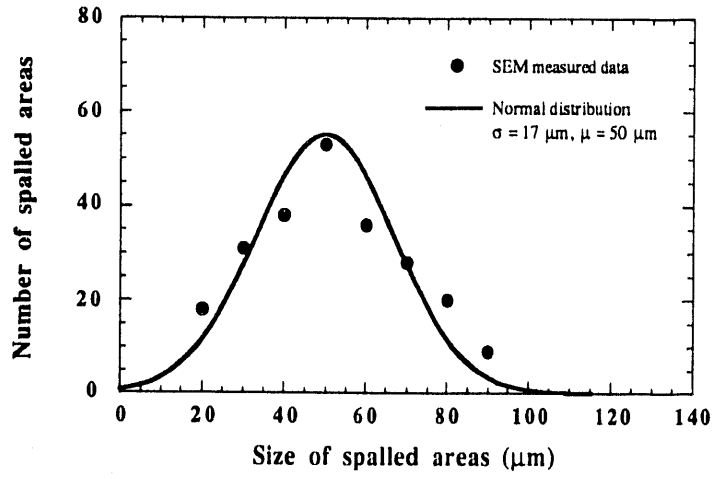

Fig. 17 The SEM measured size distribution of the spalled areas on 304 stainless steel.

Then the distribution of K_c^i can be obtained by using equation (8), the result is shown in **Fig. 18**. In the calculation, E_{ox} of the $FeCr_2O_4$ scale was taken as 270.4 GPa.[44] Using the measured average a_s and equation (8), the average (effective) value of $K_c^i \cong 4.9$ MPa$\sqrt{m}$. The calculated distribution of K_c^i can be fit to a log-normal distribution with standard deviation = 0.69 and mean = 2.19. It should be noted that for a log-normal distribution, mean and standard deviation are only scale and shape parameters, instead of being location and scale parameters as in the normal distribution.[45]

Discussion of the statistical aspects of scale cracking and spalling

The AE results show that there is a distribution of scale cracking events with cooling temperature on both Ni-30Cr alloy and 304 stainless steel. We infer from the relationship between ΔT and stress that the distribution of cracking events correlates with the product of stress and crack length, i.e., with stress intensity. SEM observation show that the spallation occurred via buckling, i.e., according to Evans' the Route II. Both of the calculated and measured spallation data follow a normal distribution. We suggest that there is a size distribution of pre-existing interfacial cracks, is the source of the distribution of the critical fracture stresses.

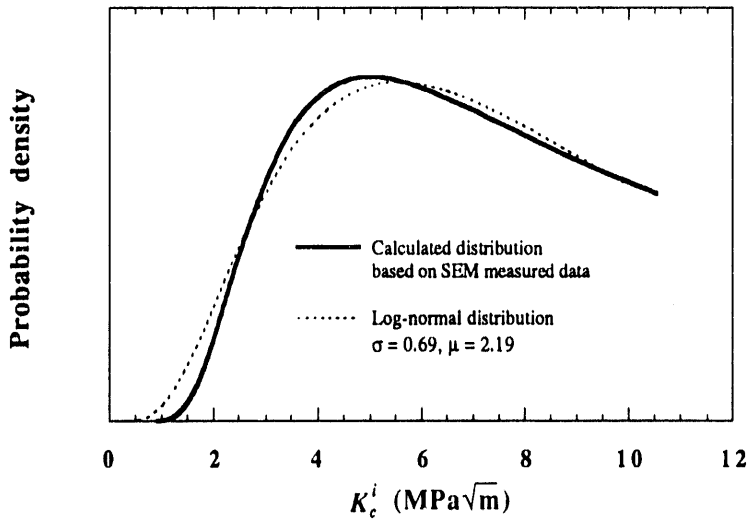

Fig. 18 The calculated distribution of the critical interfacial stress intensity factor, K_c^i, of the oxide scale formed on 304 stainless steel.

From the size distribution of the interfacial cracks one can infer a distribution of critical interfacial stress intensity, K_c^i. The results on 304 stainless steel show a log-normal distribution of calculated K_c^i. The log-normal distribution can be derived as the model for a process whose value results from the multiplication of several independent positive variates.[45] In our case, the interfacial fracture resistance, or the critical stress intensity factor, K_c^i, is a product of three terms, the stress σ, the size of interfacial flaw a and the crack geometry factor Y. When the K_c^i, value is achieved in some local region of the scale by either increasing stress (increasing the cooling amplitude ΔT) or increasing crack length (e.g., by slow crack growth at constant stress), scale spallation will occur.

This first application of statistical analysis to scale cracking, coupled with a (simple) application of fracture mechanics concepts, has led to significant new insights into scale fracture processes. For the first time, it allows a quantitative analysis of scale cracking events. It is especially encouraging that the measured spallation distributions at least roughly agree with the predicted distributions. To our knowledge, spallation distributions have neither been measured nor interpreted previously. Much further work needs to be done to verify and refine this new approach to understanding scale failure.

Micro Indentation/Scratch Technique for Measuring Scale Adhesion

The adherence of oxide scales to the metal substrate has long been of interest as a fundamental parameter important that is to understanding scale fracture and spalling. The measurement of adherence, or the energy to separate scale from metal, however, is experimentally very difficult. The current situation is that there is not available a catalog of reliable data for various metal / oxide systems, nor is there even a verified technique for such measurements. The work described below is intended to demonstrate the utility of the Micro Indentation/Scratch Technique by attempting to measure the work (energy) of adhesion of NiO on Ni and of iron oxide on Fe-3%Si. The technique has been described previously in some detail, but very briefly, a conical diamond indentor is brought into contact with the surface, then as the indentor is pushed along the surface, it is continually forced into the surface, producing a deepening scratch. The depth of penetation and the force applied to the indentor are measured with high resolution. When a piece of scale spalls, a sudden drop in force is observed. Subsequent examination of the scratch by SEM allows the spalled area to be measured. A stress and energy analysis of the region surrounding the indentor at the time of spalling allows an estimate of the energy released upon spallation. This effort is part of a broader study involving the application of a Nano-indentor to a variety of problems. For more detailed information about this technique and the interpretation of the the measurements, see:

S. K. Venkataraman, H. Huang, D. L. Kohlstedt and W. W. Gerberich, "Continuous microindentations of passivated surfaces in surface active media," Symposium M, 1993 Spring MRS Meeting, San Francisco (1993).

W. W. Gerberich, S. K. Venkataraman, H. Huang, S. E. Harvey and D. L. Kohlstedt, " The injection of plasticity by micronewton level contact forces," submitted, Phys. Rev. Lett., (1993).

S. E. Harvey, H. Huang and W. W. Gerberich, *J. Mater. Res.*, **8**, No. 6, (1993); W. Zielinski, H. Huang and W. W. Gerberich, *J. Mater. Res.*, **8**, No. 6, (1993).

S. Venkataraman, D. L. Kohlstedt and W. W. Gerberich, "Microscratch analysis of the work of adhesion for Pt thin films on NiO," *J. Mater. Res.*, **7**, No. 7, (1992).

W. W. Gerberich, S. K. Venkataraman, J. W. Hoehn and P. G. Marsh, "Fracture Toughness of Intermetallics using a micro-mechanical probe," submitted, *Metall. Trans. A*, (1993).

Micro-newton Level Indentation on Passivated Ni and Fe-3%Si Surfaces

A series of micro-newton level continuous indentation tests by monotonic loading and fatigue have been performed on a thin oxide film on a Ni substrate. The Ni substrate was

covered by a native scale having a measured thickness of about 10 nm.[46] As shown in **Fig. 19,** these tests revealed an very important phenomenon: a distinct load was repeatedly found at which a yield drop occurs with the contact area suddenly increasing by a factor of five. The identical result was also observed for Fe-3%Si single crystal surface topped with a native passivation layer of iron oxide.

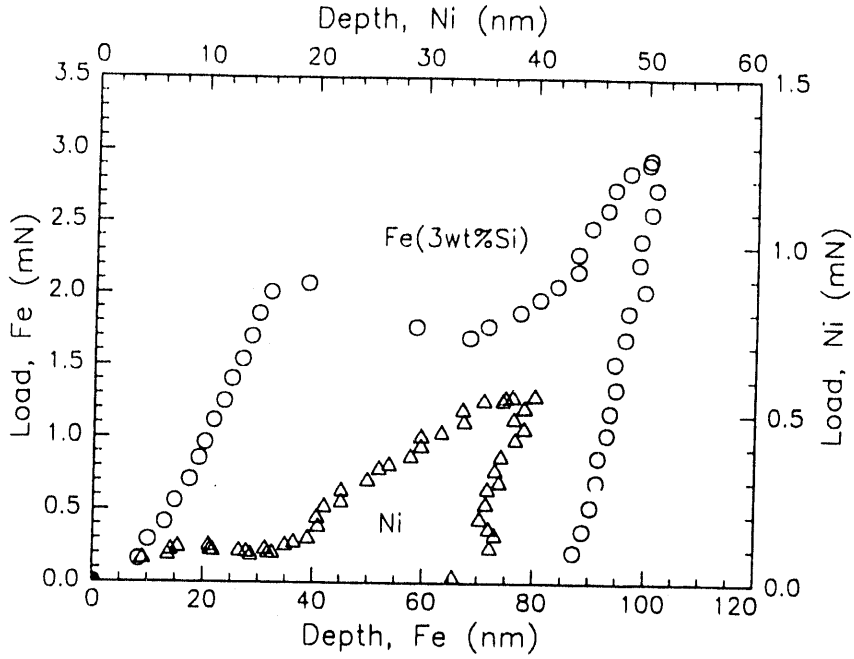

Fig. 19 Ultra light indentation of passivated Ni and Fe- 3%Si surfaces; indentation load *vs* depth for monotonic tests.

Before the indentation load reaches this yield point, the passivated surface phenomenologically behaves "elastically"; that is, the surface depression due to the indentation is totally recovered upon unloading. An elastic finite element analysis (FEA) (summarized in **Fig. 20**) predicted huge stresses of 6 GPa or greater at the scale/metal interface beneath the indenter, indicating that considerable microplasticity would be expected to occur beneath the indenter and the interface. However, on these surfaces indented with a monotonic load below the critical load, no permanent depressions were identified by atomic force microscopy (AFM). A nonlinear, elastic-plastic FEA based on conventional continuum plasticity theory was also carried out because of the suspicion that plastic yielding of the metal occurred beneath the indenter and below the oxide layer due to these huge stresses. It turned out that a considerable plastic zone would be expected to occur before the yielding point (**Fig. 20b**) according to this nonlinear continuum study.

To further explore this phenomenon, a critical experiment was then conducted on the Fe-%Si system. A series of fatigue cycles was carried out with the maximum load being below this yield point. After several cycles, a rapid excursion produced large permanent displacements below the yield point of monotonic loading. This demonstrated that the microplasticity in terms of the permanent depression does occur before the yield point and if the cycling rate is fast enough, this microplasticity can become unstable resulting in permanent deformation of the surface. This result could not be predicted by continuum models.

Prompted by the apparent inadequacy of continuum plasticity theory, a dislocation model was then developed to address the interaction between the indenter tip and dislocation loops generated at the interface and driven away by the indentation force. Following previous work[47, 48], the dislocation model revealed that before this yield point, dislocation loops are injected from the interface into the Ni substrate, where they reverse their paths, and are inhibited at the interface when the indenter is unloaded. As the indentation load increases, these dislocation loops spread out and cross-slip until the load reaches the yielding point. They force the oxide rupture by exerting a strong back force, resulting in a permanent depression on the surface. Based upon the dislocation approach, the model presented a semi-quantitative rationale of what was observed in both monotonic and fatigue tests for both Ni and Fe systems. In this sense, these ultra-thin scale films were found to provide unique characteristics to the point loading of an indentation. This new understanding, which has not been revealed in any other studies, is obviously of critical importance to physical insight concerning many micromechanical behaviors of the scale/metal interfaces. It is believed that this study provides a fundamental basis for understanding the mechanical integrity of scale/metal interfaces under abrasion and wear conditions, and may as well be applicable to erosion/corrosion phenomena.

Microscratch test on Thermally Grown NiO

A series of microscratch tests were performed on thermally grown NiO/Ni samples (**Fig. 21**. Unlike another study[49] more or less than 1 μm thick NiO scales were tested using an advanced continuous microindentation/scratch apparatus with the stylus tip radius less than 1 μm, a normal load resolution of 16 μN and a depth sensitivity of 2 nm. The surface of single crystal Ni in the <001> was first mechanically polished to 0.5 μm roughness, and then thermally oxidized in oxygen for 5 min at 900°C, followed by a very slow cooling so as to ensure scale adherence. The scale was found to have a very fine grain structure with average grain size below 1 μm and to be attached to the Ni single crystal substrate.

Due to relatively high toughness of the NiO/Ni interface, only a few cases of spallation of Ni scale pieces from the Ni substrate were found along these scratch tracks from scanning electron microscopy (SEM) observation. In one case where spallation did occur, the critical indentation load was found to be about 4.6 g, which was well below what had been anticipated from another study[49] on thick scale systems using large indentation/scratch. For the large scale scratch tests on thicker scales, over 700 g load was expected for a 1 μm thick NiO scale. This decrease in load could mostly be attributed to a decreased contact area for the conical indenter tip used (radius of the curvature R = 0.5 μm). Based on the observed spallation NiO the interfacial toughness of the NiO/Ni system was estimated to be 0.9 MPa-$m^{1/2}$, following the procedure of the determination of the work of adhesion of other thin film systems published previously[50].

Similar to what had been observed in scratch tests on other thin film systems[51], tensile type transverse cracks were always observed along scratch tracks as the indentation load reaches a critical value about 12 mN (**Fig. 22**). This transverse cracking, which might be a combination of cohesive and adhesive failures, was able to induce significant acoustic emissions signals before any purely adhesive failures occurred. Therefore, for this system, it was not straightforward to distinguish an adhesive failure from other failure modes by acoustic emission (AE) signals as reported previously[49].

(a) Elastic analysis

Mises stress levels:

1 – 300 MPa

2 – 2.29 MPa

Block drawn: 1 × 1 μm

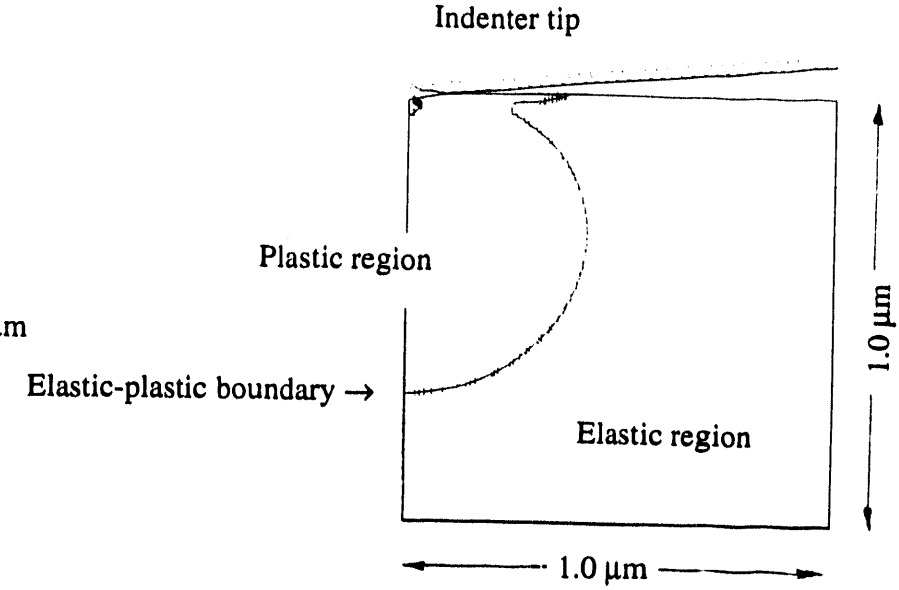

(b) Elastic-plastic analysis

Mises stress levels:

1 – 300 MPa

2 – 2.29 MPa

Block drawn: 1 × 1 μm

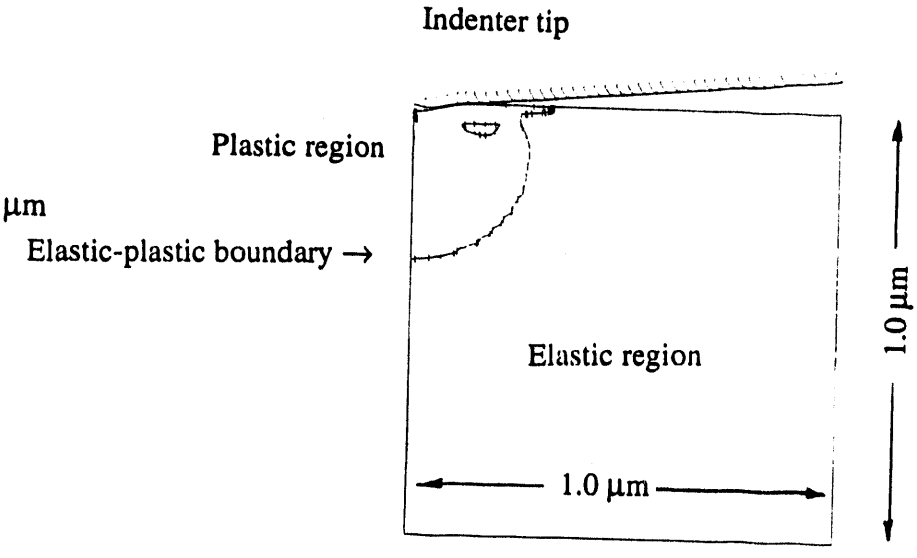

Fig.20 Finite element analyses of the microindentation of an Fe- 3%Si surface passivated with 0.02μm thick oxide (indentation profile = 0.02μm). (a) elastic analysis, (b) elastic-plastic analysis

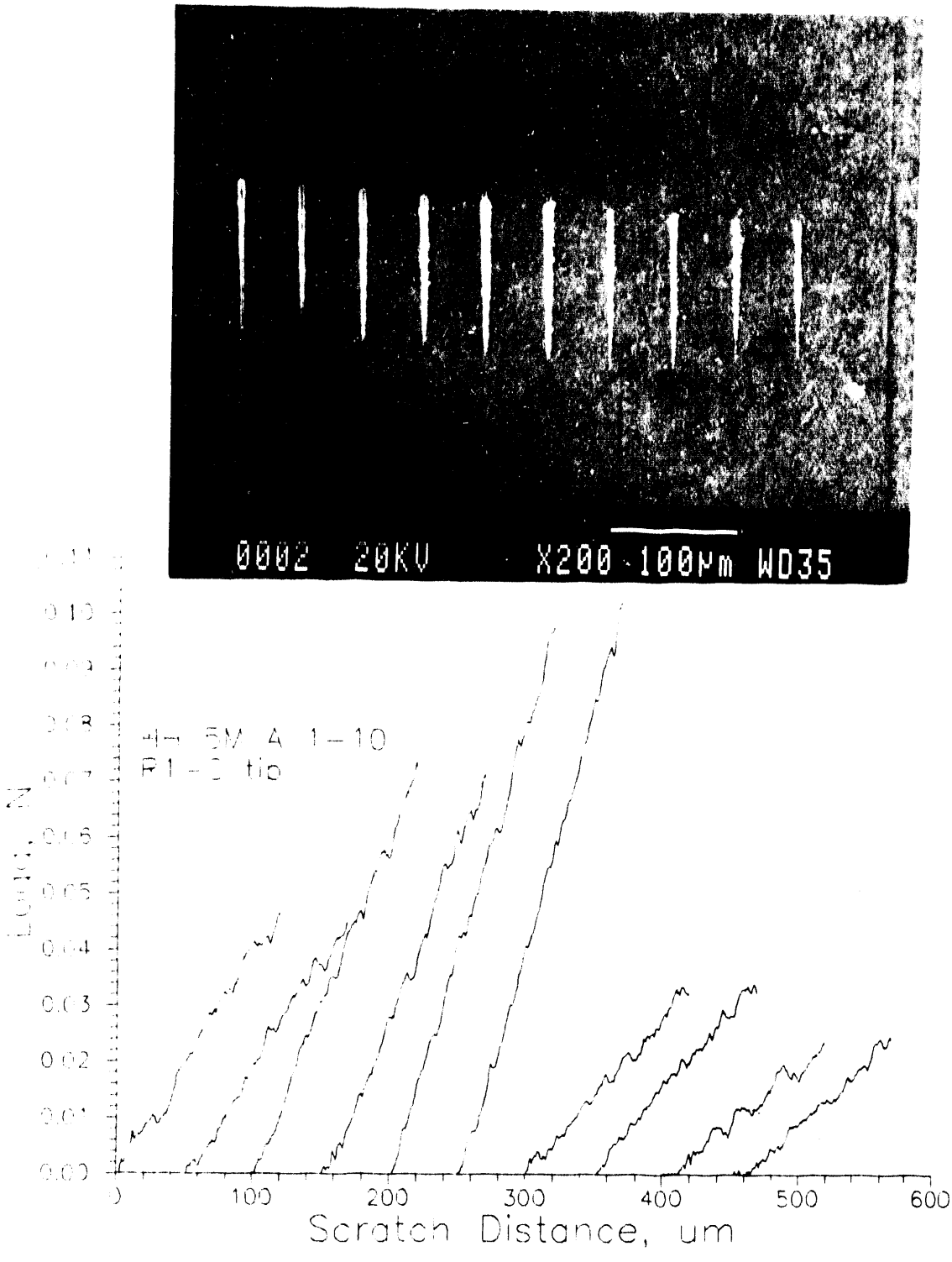

Fig. 21 SEM photo of scratches (numbered 1 - 10) on Ni/NiO and corresponding load - scratch distance curves.

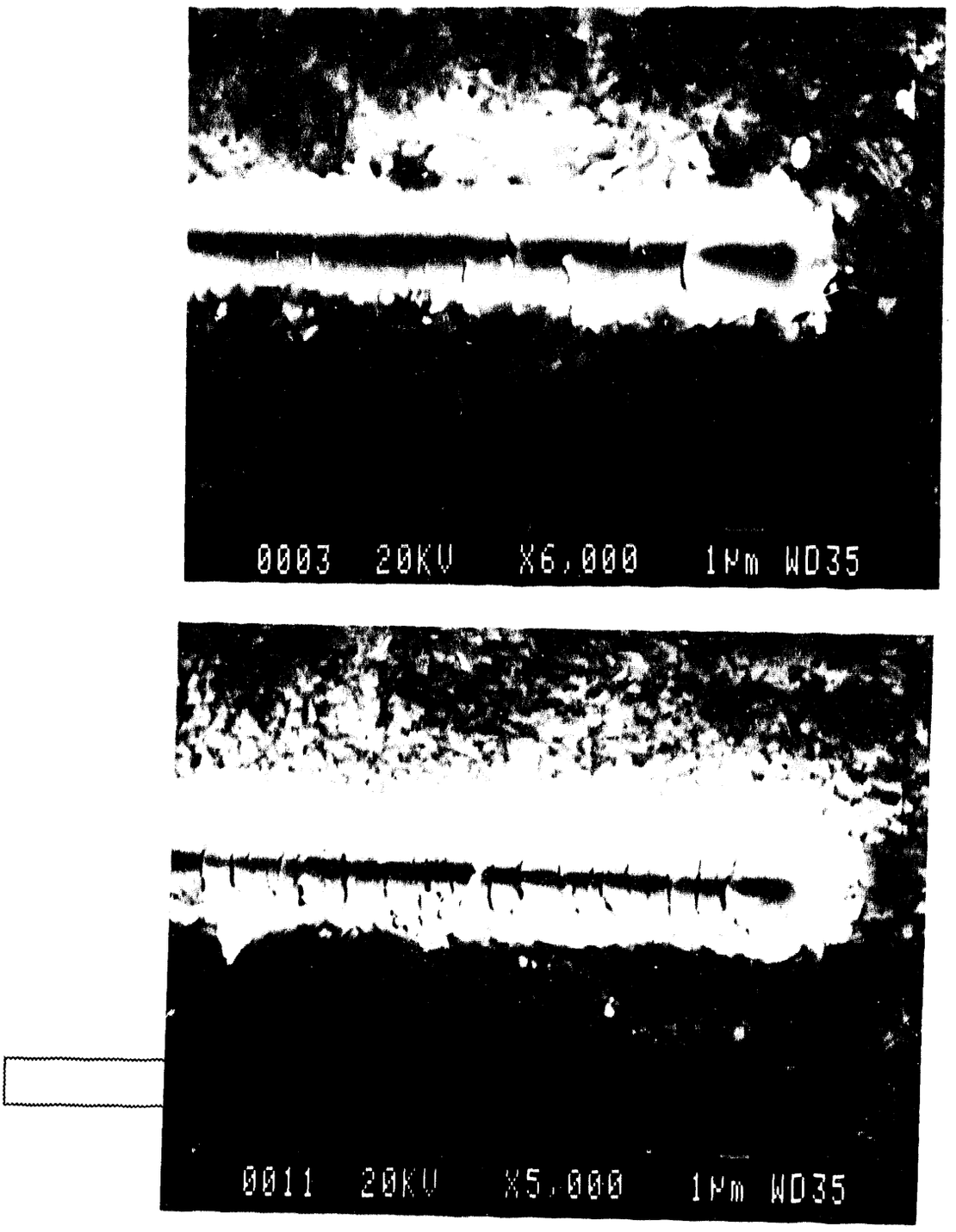

Fig. 22 SEM photos showing transverse cracks in the scratch tracks on Ni/NiO for two different normal loads: upper photo- low load, scratch No. 10 and lower photo- high load, scratch No. 2.

As noted in some studies on other thin film systems[51], the average spacing between each two adjacent cracks in NiO/Ni system was also found to decrease as the normal load of the indenter applied to the surface increased (**Fig. 23**). The variation of this periodicity or the density with the normal load can be rationalized in terms of fracture mechanics, which in turn allows us to make the first calculation of the critical energy release rate for the cracking of NiO scale and its fracture toughness. In addition, based on SEM observation and measurement of crack lengths of transverse cracks corresponding to different normal loads during the scratch, the fracture toughness of NiO scale was also calculated using the approach of a previous study[52]. The calculated toughness increases with the normal indentation load during scratch, indicating the toughening effect of the scale microplasticity induced by the scratch. As the normal load decreases, the calculated toughness tends to be below 5 MPa-$m^{1/2}$ (**Fig. 23**), which is a reasonable value compared with other oxides such as Al_2O_3. Although these are preliminary results, the implication of about 1 MPa-m for interface fracture versus 5 MPa-m for transverse cracking is that spallation would be the favored fracture mode. This result is quite consistent with the results of the acoustic emission study on Ni-30Cr and 304 stainless steel, which also concluded that crack prpogation along the oxide / metal interface was easier than through-thickness cracking.

The current scratch technique is able to provide an approximate evaluation of the adhesion or fracture toughness of a thin oxide scale. This information would enable interesting and useful comparisons to be made. For example, from this work it is known that thermally grown NiO exhibits relatively much stronger adhesion to a Ni substrate than sputtered Pt thin films adhere to NiO substrates[50]. By applying this technique to different scale/alloy systems, one would be able to make comparisons relevant to an alloy's resistance to thermal cycling based on a parameter of fundamental significance, rather than on empirical performance testing, as is now done.

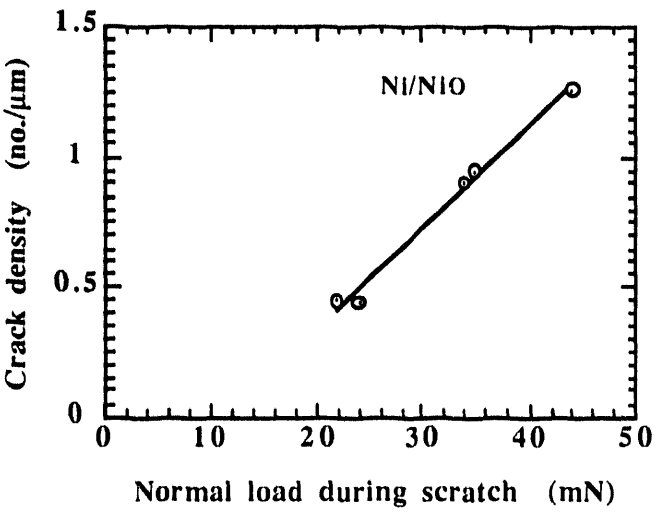

(a)

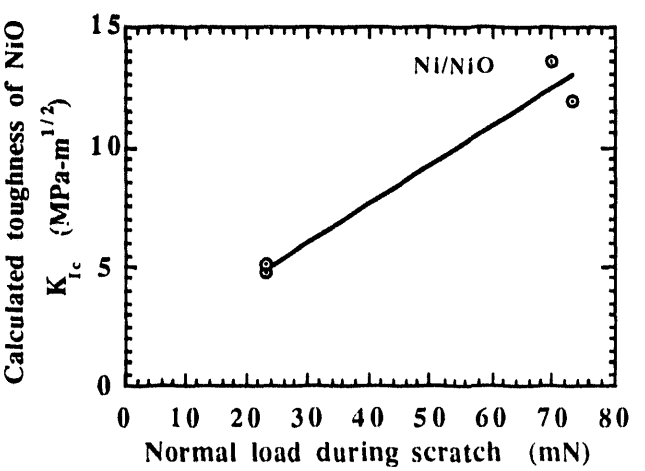

(b)

Fig. 23 (a) Correlation of cracking density in the scratch track with normal applied load; (b) Calculated fracture toughness of NiO as a function of applied normal laod.

IV. MODELING OF GROWTH STRESS DURING OXIDATION

A viscoplastic growth model was constructed to assess the stress generation during the inward growth process of the oxide scale on a thin metal plate. An oxygen transport scale growth process was selected as a first example, because the connection between scale growth and strain generation is conceptually simpler. In this model, both the growth of the new scale, accompanied by the movement of the metal/scale interface, and the viscoplastic deformation driven by growth stresses were considered simultaneously. Because a substantial modeling effort has been applied to the micro-indentor technique, we have been able to carry out only a preliminary evaluation of the growth stress model.

Unlike previous models[6, 35] for the growth stress on a flat substrate, the deformation and stress in the substrate were also considered in this model. A consistent approach was taken to incorporate the normal growth of the new scale with the interfacial misfit strain in terms of the well-known Pilling-Bedworth ratio. The model was based on a set of differential-integral equations controlling both the equilibrium of forces and the viscoplastic flow with the moving interface defined by the conventional scale growth (parabolic) equation. A simple numerical scheme of time-integration was developed to deal with the effect of a moving boundary on the growth rates of strain and stresses in the scale and substrate.

A simulation of the growth stresses during thermal oxidation of a thin Al plate was performed as a first evaluation. This simulation provided information on the time evolution of the growth stress and its gradient in Al_2O_3 layer, as well as the stress relaxation in Al substrate during a thermal oxidation process. To our knowledge, this case of examination has not been addressed by other studies.

As shown in **Fig. 24**, a compressive stress gradient appears in the Al_2O_3 scale while a homogeneous tensile stress exists in the substrate so as to maintain the force balance. The compressive stress gradient and the level of the tensile stress vary continuously as the scale grows inward at the interface. From this model, the competition of the scale growth with the stress relaxation of a scale/metal substrate system can be addressed by changing the growth condition imposed onto the interface movement. For systems other than Al_2O_3/Al, this competition might result in different growth stress patterns, which is of importance to better understand the difference of the growth stress and their mechanical stability for different metals and the alloys. It is noted that the *in situ* high temperature X-ray diffraction measurements of strains in the oxide and metal, reported in section II of the this report, will ultimately provide an important validation point for these calculations when they are applied to outward growing scales.

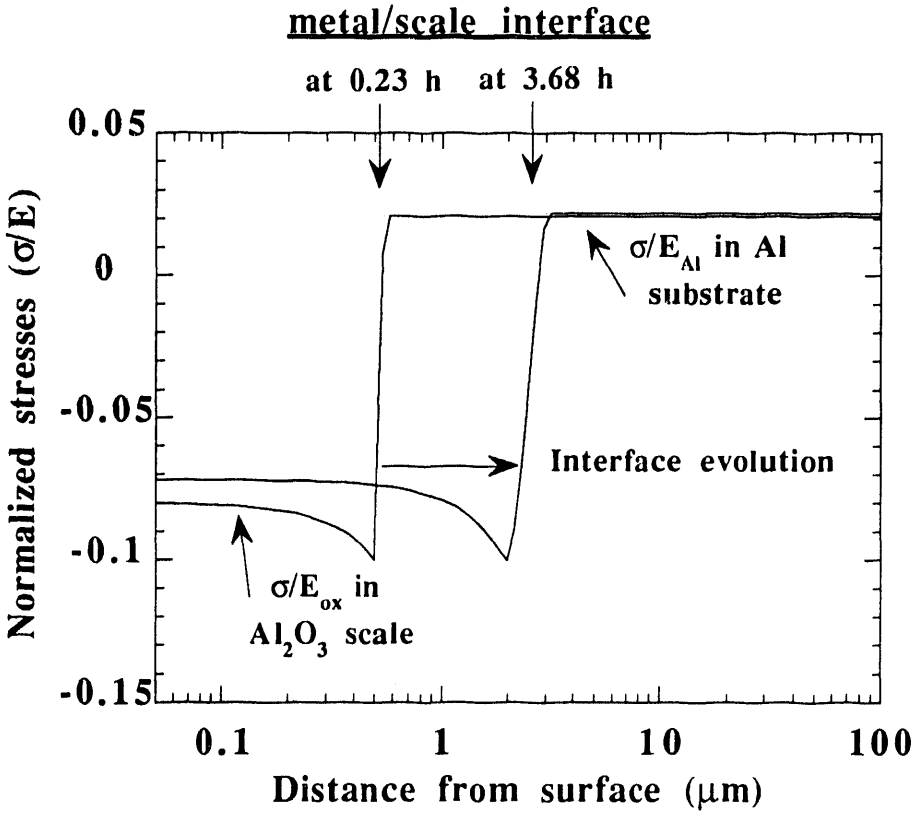

Fig. 24 Plot of normalized stresses as a function of the distance from the gas/scale interface for the oxidation of Al to Al_2O_3 at 350°.

References

1. Oxx, G. D. , Prod. Eng., **29**, (1958) p.61-63.
2. Tien, J. K. and J. M. Davidson in *Stress Effect and the Oxidation of Metals*, J. V. Cathcart, ed. The Metallurgical Society of AIME, (1974), p.201-219.
3. Stout, J. H., W. W. Gerberich, S. Lin, and M. Lii in *Fundamental Aspects of high Temperature Corrosion*, **PV86-9**, D. A. Shores and G. J. Yurek, ed. The Electrochemical Society, (1986), p.172.
4. Hsueh, C. H. and A. G. Evans , J. Am. Cer. Soc., **68**, (1985) p.241-248.
5. Birks, N. and G. H. Meier, *Introduction to High Temperature Oxidation of Metals*, Edward Arnold Publishers, Inc., London, (1983).
6. Hsues, C. H. and A. G. Evans , J. Appl. Phys., **54**, (1983) p.6672-6686.
7. Evans, H. E., G. P. Mitchell, R. C. Lobb, and D. R. J. Owen , Proc. Roy. Soc. London, **440**, (1993) p.1-22.

8. Birne, J., C. Craggs, D. J. Gardiner, and P. R. Graves , Corr. Sci., **33**, (1992) p.1-12.
9. Manning, M. I. in *Proc. Symp. on Interactions Between Corrosion and Mechanical Stress at High Temperatures,* V. Guttman and M. Merz, ed. Applied Science Publishers, Petten, Netherlands, (1980), p.323-338.
10. Evans, A. G., G. B. Crumley, and R. E. Demaray , Oxidation of Metals, **20**, (1983) p.193-216.
11. Rhines, F. N. and J. S. Wolf , Met. Trans., **1**, (1970) p.1701-1710.
12. Srolovitz, D. J. and T. A. Ramanarayanan , Oxid. Met., **22**, (1984) p.133-146.
13. Stout, J. H., D. A. Shores, J. G. Goedjen, and M. E. Armaquanqui , Materials Science and Engineering, **A120**, (1989) p.193-197.
14. Goedjen, J. G., *In-Situ Measurement of Strains in the Ni/NiO System Using a High Temperature X-ray Diffraction Technique*. Ph. D. Thesis, University of Minnesota, (1993)
15. Stout, J. H., J. G. Goedjen, Q. Guo, and D. A. Shores in *Proc. of the Sym. on X-Ray Methods in Corrosion and Interfacial Electrochemistry,* **92-1**, A. Davenport and J. G. Gordon II, ed. The Electrochemical Soc., (1992), p.101-114.
16. Goedjen, J. G., J. H. Stout, Q. Guo, and D. A. Shores , submitted to: Materials Science and Engineering, (1992).
17. Jatczak, C. F. (ed) *Automotive Engineering Congress,* Society of Automotive Engineers, Inc, New York, Paper #720242, Detroit, MI, Jan 10-14, (1972).
18. Hilley, M. E. (ed) *Automotive Engineering Congress,* Society of Automotive Engineers, Inc., New York, Paper #720241, Detroit, MI, Jan. 10-14, (1972).
19. Noyan, I. C. and J. B. Cohen, *Residual Stress Measurement by Diffraction and Interpretation*, Springer-Verlag, New York, (1987).
20. Taylor, D. , Trans. J. Brit. Ceramic Soc., **83**, (1984) p.5-9.
21. Rosenberg, S. J., *Nickel and Its Alloys*, National Bureau of Standards, Washington, D. C., (1968).
22. Pivin, J. C., J. Morvan, D. Mairey, and J. Mignot , Scripta Met., **17**, (1983) p.179-182.
23. Homma, T. and Y. Pyun , Trans. Japan Inst. Metals, Supplement, (1983) p.161-166.
24. Green, A. , Mater. Sci. Tech., **8**, (1992) p.159-162.
25. Bennett, M. J. in *High Temperature Corrosion of Advanced Materials and Protective Coatings,* Y. Saito, B. Onay, andT. Maruyama, ed. Elsevier Science Publishers, Tokyo, Japan, (1992), p.51-60.
26. Liu, C., J. L. Lebrun, and A. M. Huntz in *International Conference on Residual Stress III (ICRSIII),* H. Fujiwara, T. Abe, andK. Tanaka, ed. Elsevier Applied Science, Tokushima, Japan, (1990).

27. Ueno, T. , Trans. Japan Inst. Met., **15**, (1974) p.167-172.
28. Aubry, A., F. Armanet, G. Beranger, J. L. Lebrun, and G. Maeder , Acta Metall., **36**, (1988) p.2779-2786.
29. Luthra, K. L. and C. L. Briant , Oxid. Met., **26**, (1986) p.397-416.
30. Diot, C., P. Choquet, and R. Mevrel in *International Conference on Residual Stresses (ICRS II),* G. Beck, S. Denis, and A. Simon, ed. Elsevier Applied Science, Nancy, France, 1988, (1988), p.273-278.
31. Delaunay, D., A. M. Huntz, and P. LaCombe , Corr. Sci., **20**, (1980) p.1109-1117.
32. Moulin, G., A. M. Huntz, and J. M. Rousselet , Mater. Sci. Eng., **A120**, (1989) p.221-228.
33. Evans, H. E. and R. C. Lobb , Corrosion Science, **24**, (1984) p.209-222.
34. Evans, H. E. , Materials Science and Engineering, **A120**, (1989) p.139-146.
35. Evans, A. G. and R. M. Cannon , Materials Science Forum, **43**, (1989) p.243-268.
36. Evans, A. G. and J. W. Hutchinson , International Journal of Solids Structures, **20**, (1984) p.455-466.
37. Zhu, D. and D. A. Shores , Unpublished work.
38. Barnes, J. J., J. G. Goedjen, and D. A. Shores , Oxidation of Metals, **32**, (1989) p.449-469.
39. Timoshenko, S. and J. M. Gere, *Theory of Elastic Stability*, 2nd Edn., McGraw Hill, New York, (1961).
40. Evans, H. E. and R. C. Lobb in *'Eurocorr 87',* Dechema, Frankfurt, (1987),
41. Evans, H. E. , Materials Science and Technology, **4**, (1988) p.415-420.
42. Broek, D., *Elementary Engineering Fracture Mechanics*, 4th edition, Martinus Nijhoff Publishers, Dordrecht, (1986).
43. Stott, F. H. in *The Role of Active Elements in the Oxidation Behaviour of High Temperature Metals and Alloys,* E. Lang, ed. Elsevier Applied Science, (1989), p.3-21.
44. Simmons, G., *Single Crystal Elastic Constants and Calculated Aggregate Properties*, ed. by Claude Albritton, (1965), Southern Methodist University Press, Dallas, Texas.
45. Hahn, G. J. and S. S. Shapiro, *Statistical Models in Engineering*, John Wiley & Sons, Inc., New York, (1967).
46. Venkataraman, S. K., H. Huang, D. L. Kohlstedt, and W. W. Gerberich in *Symposium M, 1993 MRS Spring Meeting,* San Francisco, CA, (1993),
47. Harvey, S., H. Huang, and W. W. Gerberich , J. Mater. Res., **8**, (1993).
48. Zielinski, W., H. Huang, and W. W. Gerberich , J. Mater. Res., **8**, (1993).

49. Atkinson, A. and R. Guppy , Materials Science and Technology, **7**, (1991) p.1031-1041.

50. Venkataraman, S. K., D. L. Kohlstedt, and W. W. Gerberich, J. Mater. Res., **7**, (1992).

51. Wu, T. W. , J. Mater. Res., **6**, (1991).

52. Gerberich, W. W., S. K. Venkataraman, J. W. Hoehn, and P. G. Marsh , Submitted to: Met. Trans. A. (1993).

APPENDIX I

List of Pre-prints and Re-prints of Publications Relevant to this Final Progress Report

Goedjen, J.G., J. H. Stout, Q. Guo and D. A. Shores, "Evaluation of Stresses in Metal/Oxide Systems During High Temperature Oxidation by In-situ X-ray Diffraction" submitted to Materials Science and Engineering, (1992)	
Stout, J.H., J. G. Goedjen, Q. Guo and D. A. Shores, "An In-situ X-Ray Diffraction Method for the Determination of Interfacial Stresses during High Temperature Oxidation.", in *Proc. of the Sym. on X-Ray Methods in Corrosion and Interfacial Electrochemistry* , A. Davenport and J.G. Gordon II, editors, The Electrochemical Soc., (1992) **92-1**, p. 101-114.	1st page only
Goedjen, J.G., *In-Situ Measurement of Strains in the Ni/NiO System Using a High Temperature X-ray Diffraction Technique*, Ph. D. thesis, University of Minnesota, (1993).	1st page only
D. A. Shores, J. G. Goedjen, Q. Guo and J. H. Stout, "In-situ Measurement of Stresses in Oxide Scales Growing at High Temperatures", Corrosion 93, N.A.C.E., paper 254, (1993).	
Q. Guo, J. H. Stout, J. G. Goedjen and D. A. Shores, "In-situ Determination of Strains Developed During High Temperature Oxidation of Single Crystal Chromium" to be submitted to Met. Trans.	1st page only
Goedjen, J.G., D.A. Shores, and J.H. Stout, "In-Situ Strain Measurements in the Ni/NiO System During High Temperature Oxidation" to be submitted to Oxidation of Metals	1st page only
Y. Zhang and D. A. Shores, "Cracking and Spalling of Cr_2O_3 Scale Formed on Ni- 30 Cr Alloy", submitted to Oxidation of Metals, April, 1993.	
Y. Zhang and D. A. Shores, "Measurement of Oxide Scale Cracking and Spalling from 304 Stainless Steel Using Acoustic Emission", in Proc. of Symp. on Oxide Films on Metals and Alloys, Ed. B. R. MacDougall, R. S. Alwitt and T. A. Ramanarayanan, The Electrochemical Soc. 92-22, p. 250-264(1992).	1st page only
Y. Zhang and D. A. Shores, "Cracking and Spalling of Oxide Scales From 304 Stainless Steel at High Temperatures", submitted to J. Electrochem Soc., June, 1993.	
Gerberich, W.W., S. K. Venkataraman, H. Huang, S. E. Harvey, and D. L. Kohlstedt, "The Injection of Plasticity by Micronewton Level Contace Forces" Submitted to: Phys. Rev. Lett. , June, (1993).	
Venkataraman, S.K., D.L. Kohlstedt, and W.W. Gerberich, "Microscratch analysis of the work of adhesion for Pt thin films on NiO, J. Mater. Res., 7(7), (1992)	

END

DATE
FILMED
11/16/93